

Globular Cluster Systems in Nearby Dwarf Galaxies: III. Formation Efficiencies of Old Globular Clusters^{*}

Iskren Y. Georgiev^{1†}, Thomas H. Puzia², Paul Goudfrooij³ and Michael Hilker⁴

¹*Argelander Institut für Astronomie der Universität Bonn, Auf dem Hügel 71, D-53121 Bonn, Germany*

²*Herzberg Institute for Astrophysics, National Research Council, 5071 West Saanich Road, Victoria, BC V9E 2E7, Canada*

³*Space Telescope Science Institute, 3700 San Martin Drive, Baltimore, MD 21218, USA*

⁴*European Southern Observatory, Karl-Schwarzschild-Str. 2, 85748 Garching bei München, Germany*

April 2010

ABSTRACT

We investigate the origin of the shape of the globular cluster (GC) system scaling parameters as a function of galaxy mass, i.e. specific frequency (S_N), specific luminosity (S_L), specific mass (S_M), and specific number (\hat{T}) of GCs. In the low-mass galaxy regime ($M_V \gtrsim -16$ mag) our analysis is based on *HST/ACS* observations of GC populations of faint, mainly late-type dwarf galaxies in low-density environments. In order to sample the entire range in galaxy mass ($M_V = -11$ to -23 mag = 10^6 – $10^{11} L_\odot$), environment, and morphology we augment our sample with data of spiral and elliptical galaxies from the literature, in which old GCs are reliably detected. This large dataset confirms (irrespective of galaxy type) the increase of the specific frequencies of GCs above and below a galaxy magnitude of $M_V \simeq -20$ mag. Over the full mass range, the S_L –value of early-type galaxies is, on average, twice that of late-types. To investigate the observed trends we derive theoretical predictions of GC system scaling parameters as a function of host galaxy mass based on the models of Dekel & Birnboim (2006) in which star-formation processes are regulated by stellar and supernova feedback below a stellar mass of $3 \times 10^{10} M_\odot$, and by virial shocks above it. We find that the analytical model describes remarkably well the shape of the GC system scaling parameter distributions with a universal *specific GC formation efficiency*, η , which relates the total mass in GCs to the total galaxy halo mass. Early-type and late-type galaxies show a similar mean value of $\eta = 5.5 \times 10^{-5}$, with an increasing scatter towards lower galaxy masses. This can be due to the enhanced stochastic nature of the star and star-cluster formation processes for such systems. Some massive galaxies have excess η values compared to what is expected from the mean model prediction for galaxies more luminous than $M_V \simeq -20$ mag ($L_V \gtrsim 10^{10} L_\odot$). This may be attributed to a very efficient early GC formation, less efficient production of field stars or accretion of predominantly low-mass/luminosity high- η galaxies, or a mixture of all these effects.

Key words: galaxies : dwarf – galaxies : irregular – galaxies : star clusters

1 INTRODUCTION

One of the very first stellar systems to form in the early Universe are old globular clusters (GCs), which are observed in galaxies of all morphological types. Globular clusters are massive agglomerations of gravitationally bound stars, the majority of which formed almost simultaneously out of gas

with similar chemical composition. As fossil records of the first star formation episodes of their host galaxies, the distribution of their integrated properties (age, mass, metallicity, structural parameters) as well as the general properties of all GCs in a galaxy (total numbers, spatial and dynamical distributions) hold important clues to the initial physical conditions at which they have formed and evolved. For that reason, the global properties of globular cluster systems (GCSs) have long been recognized as promising tools to study the major galaxy star formation episodes and to serve as observational constraints to differentiate between various models of galaxy formation (Kissler-Patig 2000; van

^{*} Partly based on archival data of the NASA/ESA *Hubble Space Telescope*, which is operated by AURA, Inc., under NASA contract NAS 5–26555.

[†] E-mail: iskren@astro.uni-bonn.de

den Bergh 2000; Harris 1991, 2003; Brodie & Strader 2006, and references therein).

One of the most commonly used parameters to describe GCSs is the *specific frequency* (S_N), i.e. the number of GCs per unit galaxy luminosity. In essence, S_N measures the formation efficiency of GCs relative to field stars. GCs and field stars are linked through the dissolution of star clusters due to various mechanisms (e.g. tidal shocks, cluster relaxation), which shapes the initial power-law to the observed, present-day Gaussian globular cluster luminosity function (GCLF, see e.g. Fall & Zhang 2001; Goudfrooij et al. 2004, 2007; Gieles et al. 2006; McLaughlin & Fall 2008; Kruijssen & Portegies Zwart 2009; Elmegreen 2010, and references therein). The S_N parameter was initially introduced by Harris & van den Bergh (1981) as a measure of the richness of GCSs in elliptical galaxies. Since then S_N has been applied by numerous studies to galaxies of different morphological types from early-type, quiescent ellipticals to actively star-forming, late-type spirals, irregulars, and interacting/merger galaxies, covering the entire range in galaxy mass (from giants to dwarfs) and environments (from galaxies in dense clusters to such in loose groups and in the field). Wide-field ground-based and deep Hubble Space Telescope (HST) studies show that the S_N value varies *greatly* among galaxies, particularly among the most luminous ellipticals and low-mass dwarf galaxies (e.g. Harris 1991, 2001; Wehner et al. 2008; Peng et al. 2008). Spiral galaxies tend to show much less scatter in their S_N , with values in the range 0.5–2 (Ashman & Zepf 1998; Goudfrooij et al. 2003; Chandar et al. 2004; Rhode et al. 2007). The general trend observed for early-type dwarf elliptical (dE) galaxies is that their average S_N value increases with decreasing galaxy luminosity from a few to a few tens (Durrell et al. 1996; Miller et al. 1998; Miller & Lotz 2007; Peng et al. 2008). It was shown recently that a similar behavior of S_N holds for late-type dwarfs (dIrrs, Seth et al. 2004; Olsen et al. 2004; Sharina et al. 2005; Georgiev et al. 2008; Puzia & Sharina 2008). Conversely, in the high-mass galaxy regime, a significant increase of the S_N values is observed for the most luminous galaxies (gEs and cDs, e.g. Rhode et al. 2005; Peng et al. 2008; Harris et al. 2009). As the stellar populations (colours and integrated light spectral indices) of the latter galaxies are not significantly different from galaxies 1-2 mag fainter, such an upturn in the S_N distribution implies that the assembly history of the most massive galaxies must have been different from those of less massive galaxies.

The overall trend for S_N is that with increasing galaxy luminosity from $M_V \simeq -11$ mag to $M_V \simeq -20$ mag, S_N decreases from the range $\sim 0-100$ to $S_N \sim 0.5-3$, respectively. For galaxies more luminous than $M_V \simeq -20$ mag the S_N increases again (to ~ 10).

To explain the increasing fraction of GCs over field stars in the most massive galaxies several studies suggested that the mass in GCs is proportional to the total gas mass supply (West et al. 1995; Blakeslee et al. 1997; Blakeslee 1999). In particular, McLaughlin (1999) investigated the S_N behavior for the entire early-type galaxy mass range, from giants to dwarfs. He showed that the enhanced S_N for the most massive galaxies considered in his sample (NGC 1399, M87, M49) can be accounted for if the mass in GCs is normalized to the total baryonic mass of the host (stellar plus the hot X-ray emitting gas), implying a constant

baryonic GC formation efficiency $\epsilon = 0.26\%$. The parameter ϵ represents the efficiency of converting baryonic matter into GCs, $\epsilon \equiv \mathcal{M}_{\text{GCS}}/\mathcal{M}_b$. However, as suggested by Blakeslee et al. (1997) and Blakeslee (1999), perhaps more fundamental is the ratio between the mass in GCs and the *total* galaxy halo mass \mathcal{M}_h , (i.e., $\eta_h \equiv \mathcal{M}_{\text{GCS}}/\mathcal{M}_h$) for which they obtain $\eta_h \simeq 1.71 \times 10^{-4}$. More recently, Kravtsov & Gnedin (2005) in a high-resolution cosmological simulation for galaxies with $\mathcal{M}_h > 10^9 \mathcal{M}_\odot$ find $\mathcal{M}_{\text{GCS}} = 3.2 \times 10^6 \mathcal{M}_\odot (\mathcal{M}_h/10^{11} \mathcal{M}_\odot)^{0.13}$, which predicts $\epsilon_h = (2-5) \times 10^{-5}$. Assuming a cosmological baryon fraction $f_b = 0.17$ (Hinshaw et al. 2009) brings the observed and theoretically predicted values of the GC formation efficiency to a common value of $\sim 10^{-5}$ (see Sect. 4.3). Following up on the idea of the proportionality between the mass in GCs and the host halo mass using a statistical stellar-halo mass relation from Λ CDM simulations, recent studies with much larger galaxy samples find a good approximation to the data (Peng et al. 2008) and a similar result for the GC formation efficiency ($\eta_h = 7 \times 10^{-5}$, Spitler & Forbes 2009). In the low-mass galaxy regime, Peng et al. (2008) find evidence for an environmental bias: the majority of dwarf galaxies with relatively high S_N at a given total luminosity lie within a projected radius of ~ 1 Mpc from M87, the central giant elliptical in the Virgo galaxy cluster. The study of Miller & Lotz (2007) finds a consistent trend of increasing GC mass fraction with decreasing host galaxy mass for Virgo dwarf elliptical galaxies. Using the McLaughlin (1999) correction for $\mathcal{M}_{\text{gas}}^{\text{init}}/\mathcal{M}_{\text{star}}^{\text{init}}$, Miller & Lotz were able to match the trend seen in their observations.

Investigating the increasing S_N with decreasing galaxy mass below $\mathcal{M}_* < 3 \times 10^{10} \mathcal{M}_\odot$, Forbes (2005) used the feedback models of Dekel & Woo (2003) which predict $\mathcal{M}/L \propto \mathcal{M}^{-2/3}$, and found qualitative agreement with the observations. However, the normalization of this relation remained unconstrained, so that actual GC formation efficiency values ϵ_h could not be determined. This quantitative derivation of GC system scaling relations as a function of galaxy mass is one of the goals of this work by including predictions from the latest Dekel & Birnboim (2006) models which include shock-heating regulated star formation for $\mathcal{M}_* > 3 \times 10^{10} \mathcal{M}_\odot$. In Section 2 we briefly introduce the galaxy sample used in this study and access contamination. The analysis of the fractions of GCs in late-type dwarf galaxies along with complementing data from the literature is presented in Section 3. In Section 4 we discuss the observed trends of the various GCS scaling relations, the specific GC formation efficiency η , and implications for galaxy formation scenarios. Combined with dynamical mass measurements of massive and dwarf galaxies from the literature we normalize the models (Sect. 4.2.1) and find a good description of the observed behavior of the frequencies of GCs as a function of galaxy luminosity with a common value of the GC formation efficiency parameter. Using the derived analytical expressions describing the behavior of the specific GC system scaling parameters as a function of galaxy luminosity we discuss (in Sect. 4.4) the predictions of a simplistic satellite galaxy accretion model as a function of galaxy luminosity. Our final conclusions are summarized in Sect. 5.

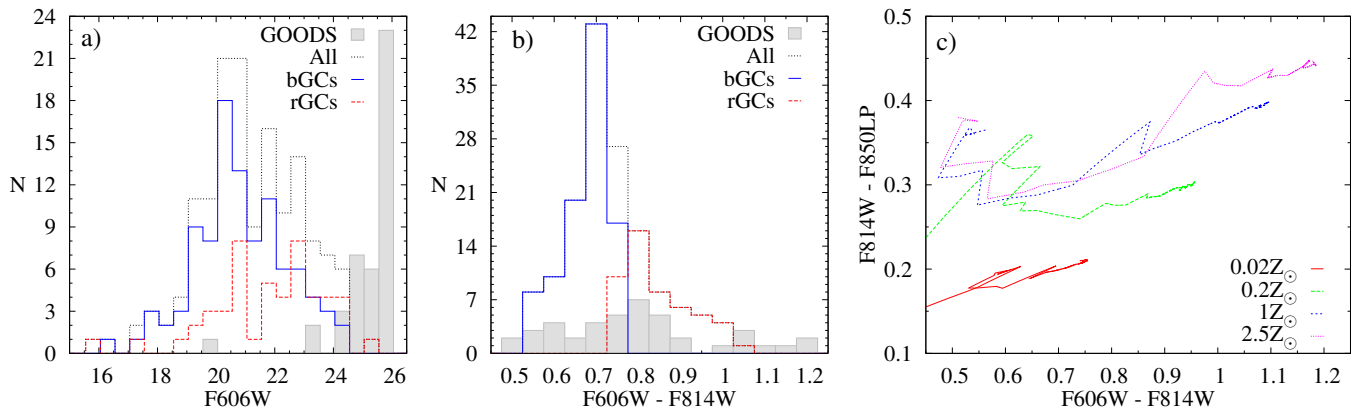


Figure 1. Contamination analysis. **Panel a)** and **b)** show a comparison between the apparent luminosity and color distributions for GC candidates in our sample (all, blue and red GC samples with dotted, solid and dashed histograms) and those for sources in the GOODS survey (filled histograms) selected similarly to our initial GC candidates selection. Applying identical criteria for the selection of contaminants from the GOODS catalog was not possible due to the lack of F814W-band imaging in the latter. Magnitude and object morphological selection was based on the GOODS F606W-band measurements and an F606W–F850LP color cut derived from a comparison with SSP models, to include the entire range in metallicity at ages > 1 Gyr, matching the F606W–F814W color selection. Transformation from F606W–F850LP to F606W–F814W color requires knowledge of the object metallicity. This is well seen in the **panel c)** where we show the F606W–F814W versus F814W–F850LP Galev SSP model tracks (Anders & Fritze-v. Alvensleben 2003) for a range of metallicities indicated in the legend. For an approximate comparison, we applied a shift of 0.25 mag to the GOODS F606W–F850LP color distribution in panel **b)**.

2 DATA

2.1 HST/ACS imaging data

The analysis of the specific frequencies of mostly late-type dwarf galaxies in this study is based on HST/ACS archival data from programs SNAP-9771 and GO-10235 (PI: I. Karachentsev), and GO-10210 (PI: B. Tully). These snapshot surveys provide Tip-of-the-Red-Giant-Branch distances to all dwarf galaxies in the studied sample (Tully et al. 2006; Karachentsev et al. 2006, 2007), and deep observations to study the GC systems of the dwarf galaxies. Our sample of dwarf galaxies consists of 55 dIrrs, 3 dEs, 5 dSphs, and 5 Sm galaxies in the field environment, either in loose associations of dwarfs or in remote halo regions of nearby groups (Sculptor, Maffei 1 & 2, IC 342, M 81, CVn I cloud). We have detected old GCs in 38 dwarf galaxies (cf. Table 1 in Georgiev et al. 2009a). Most of the dwarfs have apparent diameters smaller than the HST/ACS field of view which provides us with a good sampling of their GCSs. The GC numbers of two dwarf Sm galaxies from GO-10210 (NGC 784 and ESO 154-023) and three Sm galaxies from SNAP-9771 and GO-10235 (ESO 274-01, NGC 247, and NGC 4605) have been corrected for spatial incompleteness. Details on the data reduction, cluster selection and photometry, completeness and total galaxy luminosity are described in detail in Georgiev et al. (2008, 2009a).

2.2 Contamination Analysis with HUDF and GOODS Data

An important aspect which can affect the statistics of our analysis, especially for the faintest dwarf galaxies with fewer detected GC candidates, is the issue of background contamination. In Georgiev et al. (2008) we used the ACS Hubble Ultra Deep Field (HUDF) to select objects with the same magnitude and morphological selection criteria as our sam-

ple GCs. Our analysis showed that the depth and resolution of the ACS images allowed us to exclude background contamination among the blue GC candidates, even at the previously adopted redder cut between blue and red objects at $(V - I) = 1.1$ mag. In our latest studies we have adopted a bluer cutoff between blue and red GC candidates at $(V - I)_0 = 1.0$ mag which is the selection for the current study as well. For a more conservative analysis and for further narrowing the possibility of contamination we selected for this study GC candidates in the color range $0.7 < V - I < 1.4$ mag, in accordance with the colors of Galactic and old LMC GCs.

In order to double-check the contamination level and avoid selection biases due to cosmic variance, we have accessed the latest version v2.0 of the GOODS catalog (Great Observatories Origins Deep Survey, Giavalisco et al. 2004). GOODS is a deep imaging survey with HST/ACS in four bands (B_{F435W} , V_{F606W} , i_{F775W} , z_{F850LP}) of two locations in the north and south sky covering a total of ~ 320 arcmin². We matched all sources with photometry in F606W and F850LP with a tolerance of 1 pixel for both GOODS-N and GOODS-S catalogs. This yields a total number of 39 432 and 33 955 sources, respectively.

We analyze the contamination in a similar manner as in Georgiev et al. (2008) by employing morphological information from the GOODS catalog and selecting sources with $19 < F606W < 26$ mag, $2 < FWHM_{F606W} < 9$ and ellipticity in the range $0 - 0.15$, identical to our F606W images. By applying the same objects selection strategy as for our science images on the entire high-level science GOODS v2.0 imaging data¹ we confirmed the morphological selection. To constrain the selection of GOODS sources in a similar $V - I$ color range, as the selection of our GC candidates,

¹ Retrieved from <http://archive.stsci.edu/prepds/goods/> and piped through the same analysis routines of F606W images.

we used the F606W–F850LP color. Observations of other galaxies, Galactic and Magellanic Cloud Clusters have Johnson/Cousins colors in the range $0.7 < V - I < 1.4$ mag, which we convert using the Galev SSP models (Anders & Fritzev. Alvensleben 2003) to $0.74 < F606W - F850LP < 1.55$ for ages older than $\gtrsim 1$ Gyr for the entire metallicity range. As a result, 18 and 24 objects passed the above selection criteria for the North and South GOODS fields, respectively. Combined and normalized to the total GOODS survey area of 320 arcmin^2 leads to an upper limit of the total contamination density of $\rho \approx 0.13$ objects per arcmin^2 , i.e. ~ 1.5 objects in a single ACS field with an area of 11.33 arcmin^2 . In total we have 30 galaxies with blue GC detections (see Sect. 3.1), i.e. $\sim 340 \text{ arcmin}^2$ which is comparable to the total area of the GOODS fields. Thus, virtually no scaling to the number of contaminating objects is required for the direct comparison shown in Figure 1. The luminosity and color distributions of all contaminating sources are shown in panels a) and b). The magnitude difference between F814W and F850LP shown in panel c) is in the range $0.15 - 0.45$ mag. This shows that without knowing the object metallicity it is not possible to derive precise information about the contamination as a function of color. To partially account for this difference and ease the comparison we shifted the color distribution of GOODS objects in Figure 1 b) by 0.25 mag. The luminosity distribution of background objects reveals that the contamination in our entire GCs sample is of the order of $\sim 5 - 6$ among the faintest, barely resolved GC candidates. This additional analysis of two different sky regions with deep ACS imaging confirms the expected low level of contamination. Section 3.1.1 discusses the implications of this result.

3 ANALYSIS

3.1 Specific Frequency

The globular cluster specific frequency is defined as

$$S_N = N_{GC} \times 10^{0.4(M_V + 15)} \quad (1)$$

(Harris & van den Bergh 1981) and is a measure of the ratio of the formation efficiencies of star clusters to field stars. It describes how likely it is for a given galaxy to have formed star clusters that survived the various cluster disruption mechanisms until today. Two factors affect the S_N -values in late-type dIrr galaxies: the recent star formation activity of the host galaxy affects M_V while the dynamical evolution history of its GC system affects N_{GC} .

In particular, for our sample galaxies the influence of changes in galaxy luminosity is more significant for late-type dwarf galaxies for which the present-day starburst activity can boost their luminosity, causing a decrease in the S_N values. Formation and subsequent dynamical evolution of GCs in low-mass galaxies (where fewer clusters are formed) leads to stochastic fluctuations in N_{GC} which can lead to an increased dispersion of S_N among such dwarfs, which is indeed observed. In addition, the stochastic nature of the field-star formation history for dIrrs (e.g. Weisz et al. 2008) can introduce additional scatter.

In spite of this, the field star and star-cluster formation efficiencies generally appear to be closely correlated as it is observed that the ratio of cluster to star formation rates

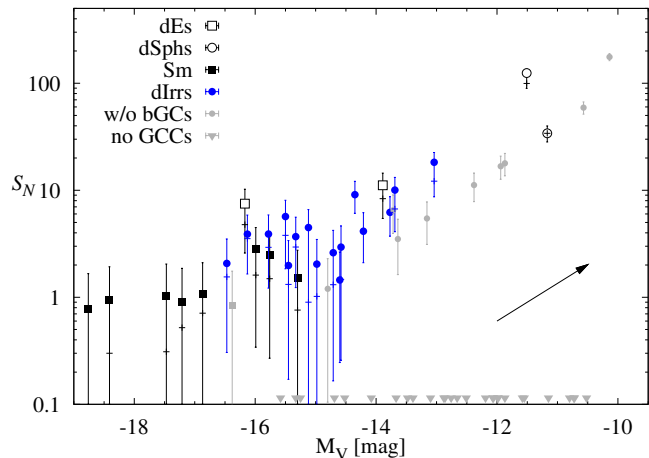


Figure 2. Globular cluster specific frequency, S_N , versus absolute galaxy magnitude, M_V , for all dwarf galaxies in our sample. Symbols are the bGC+rGC estimates of the S_N values for various galaxy types, while plus signs indicate the values based on the bGC population only. Grey triangles at the bottom of the plot represent galaxies in which no GCCs were detected. The black arrow indicates the change of the S_N value due to passive evolutionary fading of the galaxy light by $\Delta M_V = 1.5$ mag (from 3 to 14 Gyr at LMC metallicity).

(SFR) is nearly constant (e.g. Lada & Lada 2003; Lamers & Gieles 2008; Gieles & Bastian 2008) and independent of the present-day SFR (Bastian 2008). In addition, the constant ratio between star-cluster mass and the mass in field stars at the end of violent relaxation² (i.e. the bound cluster-to-field stellar mass ratio) may be evidence for a nearly universal distribution function of the *local* star formation efficiency (Parmentier & Fritze 2009).

3.1.1 Specific frequencies of dwarf galaxies in our sample

We compute two S_N values for our sample of GC candidates selected from Georgiev et al. (2008, 2009a) in the color range $0.7 < V - I < 1.4$ mag. First using the number of blue GCs and second the total number of GCs: blue GCs + red GCs (red GCs have $(V - I)_0 > 1.0$ mag), together with the total V -band galaxy magnitudes derived in Georgiev et al. (2008, 2009a). The calculated S_N values for all dwarf galaxies in our sample are shown in Figure 2 and listed in Table 1. The contamination analysis in Section 2.2 suggests that red GC candidates with $1.0 < (V - I) < 1.4$ can not be fully accounted for by contamination in our sample galaxies. This is puzzling because the existence of such red, metal-rich GCs in low-mass dwarf galaxies is not expected. The fraction of red GCs in early-type galaxies decreases with decreasing galaxy luminosity and becomes negligible for the faintest dEs (cf Fig. 4 and 10 in Peng et al. 2006). Theory suggests that red, metal-rich clusters are believed to form either in major galaxy mergers (e.g. Ashman & Zepf 1992) or in a multi-phase collapse of

² The end of violent relaxation, when the dynamical response of a cluster to the expulsion of its leftover star forming gas is completed, typically takes place at an age between 10 and 50 Myr and depends on the external tidal field and the proto-cluster crossing-time (see Fig. 4 in Parmentier 2009).

a massive galaxy (Forbes et al. 1997; Pipino et al. 2007). Both channels are unlikely to occur in low-mass systems. Observationally, extinction within the galaxy can lead to a redder colour. Taking the Magellanic Clouds as a proxy for the dwarfs in our sample, the expected internal reddening is in the range $0 < E(V-I) < 0.13 \text{ mag}$ ³. The radial distribution of the bGCs and rGCs in our sample galaxies are indistinguishable from each other. They are distributed mostly within 1-2 pc projected distance from the galaxy center, i.e. $\sim 1 \times R_{\text{eff}}$ (Georgiev et al. 2009b). Therefore, some internal reddening can be expected among the GCs in our sample. Red colors could arise if clusters have ages in the range 1 – 3 Gyr where AGB stars are in their thermal-pulsation phase (TP-phase) which affects the integrated cluster color. Comparison with population synthesis models (e.g. Maraston 2005; Leitherer et al. 1999) shows that for that age range the integrated cluster colour can reach $V-I < 1.4 \text{ mag}$ for even as low metallicities as 0.2 to 0.4 Z_{\odot} . However, whether reddening or younger ages are affecting the colors of GCs in our sample, or whether they are background contaminants will require spectroscopic or near-IR follow-up observations to establish their accurate metallicities and membership.

In order to minimize the effects on the S_N from the uncertain nature of the rGCs in our subsequent analysis, we consider *only* dwarf galaxies which contain blue GC candidates. There are eight galaxies (20%) with only red GCs which are treated as galaxies with null GC detections. The lack of bGCs does not necessarily mean that some of the rGCs cannot be real GCs due to the effects discussed above. Therefore, given these uncertainties, our S_N s represent a conservative *lower* value for faint late-type galaxies. In Section 4.2.2 we discuss the implications and limitations of the presence of rGCs for the model we are testing.

Overall, the observed trend of increasing S_N with decreasing host galaxy luminosity holds for the entire sample, and in particular for dIrrs. Because of their small sample size the trends for dEs/dSphs and Sm galaxies are less conclusive from our data alone. Grey triangles show galaxies where no GC candidates are detected. Their S_N values were adjusted for illustrative purposes only. Notably, Figure 2 shows that for low-luminosity galaxies the difference between total S_N (where the rGCs sample can include background contaminants) and blue GC S_N (the most trustworthy value) differ a little quantitatively, but not significantly in the qualitative sense due to the logarithmic scaling. Thus, the observed general trend of increasing S_N value with decreasing galaxy luminosity is present even if only S_N values calculated from the blue GCs (bGCs) are considered.

It is important to note that all S_N values for the late-type dwarfs represent their present-day values. Passive evolutionary

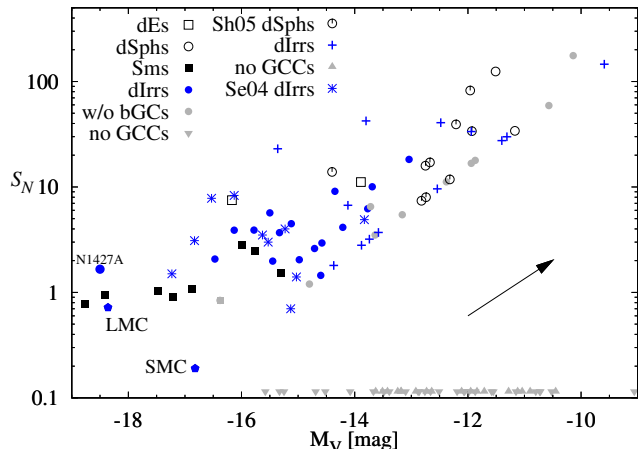


Figure 3. GC specific frequency as a function of absolute galaxy magnitude for dwarf galaxies at low density environment from Sharina et al. (2005); Georgiev et al. (2008, 2009a) and dIrrs in Virgo and Fornax cluster Seth et al. (2004); Georgiev et al. (2006). Dwarf irregular galaxies are shown with solid circles, plus signs and asterisks; dSphs with open and dashed-open circles; Sms with solid squares. With solid pentagons we show S_N values of the best studied GC systems in nearby dIrrs – the LMC and SMC. Grey triangles at the bottom of the plot represent galaxies in which no GCCs were detected. The arrow indicates passive evolutionary fading as in Figure 2.

lutionary fading of the integrated galaxy light will increase the S_N values by a factor of 2 to 16 for our dIrr and Sm galaxy sample (assuming $N_{\text{GC}} = \text{const.}$). This is shown by an arrow in Figure 2, which indicates the change in S_N if a galaxy passively fades due to stellar evolution by $\Delta M_V = 1.5 \text{ mag}$. This corresponds to an evolution from 3 to 14 Gyr at LMC metallicity as inferred from SSP models (e.g. Bruzual & Charlot 2003).

3.1.2 Comparison of S_N values of late-type dwarf galaxies

In Figure 3 we compare the S_N values of our sample dwarfs with those of late-type dwarfs from Sharina et al. (2005), all in field environment, and Virgo and Fornax cluster dIrrs from Seth et al. (2004) and Georgiev et al. (2006), as well as the Magellanic Clouds. It is clearly seen that, combined with the data from the literature, we observe a general trend of increasing S_N with decreasing galaxy luminosity for dIrrs. Such a trend has been previously observed for early-type dEs (e.g. Miller et al. 1998; Strader et al. 2006). The dIrrs in our sample are systematically brighter than dSphs by $\sim 3 \text{ mag}$, indicating younger ages. As mentioned above, a simple picture of passive evolutionary fading of the dIrrs can shift their S_N values toward the dSphs region, parallel to the average trend. This supports the notion that if the number of GCs remains unchanged the high- z analogs of present-day dIrrs might be the progenitors of the more evolved dSphs/dEs (e.g. Miller et al. 1998; Seth et al. 2004).

To investigate the formation efficiency of GCs as a function of galaxy luminosity, we extend the galaxy mass range and morphology by including data from the literature. In Figure 4 we compare the specific frequencies of the dwarf galaxies discussed above with those of early-type galaxies in

³ The total $E(B-V)$ value for old LMC GCs is in the range 0.083 – 0.213 mag for NGC 1898 and NGC 1841 (McLaughlin & van der Marel 2005). Corrected for the median Galactic foreground reddening toward LMC of $E(B-V) = 0.075 \text{ mag}$ (Schlegel et al. 1998), leads to $E(B-V) = 0.008$ and 0.138 mag, i.e. $E(V-I) = 0.009$ and 0.164 mag internal reddening for the LMC. The same analysis for the only old SMC GC, NGC 121, gives $E(B-V) = 0.109 \text{ mag}$ or $E(V-I) = 0.130 \text{ mag}$. The LMC GCs above are at $R = 0.6^\circ$ and 14.9° projected distance from the center of the LMC (van den Bergh & Mackey 2004). $m-M = 18.5 \text{ mag}$ (50.118 kpc) to the LMC yields 0.5 and 13.3 kpc.

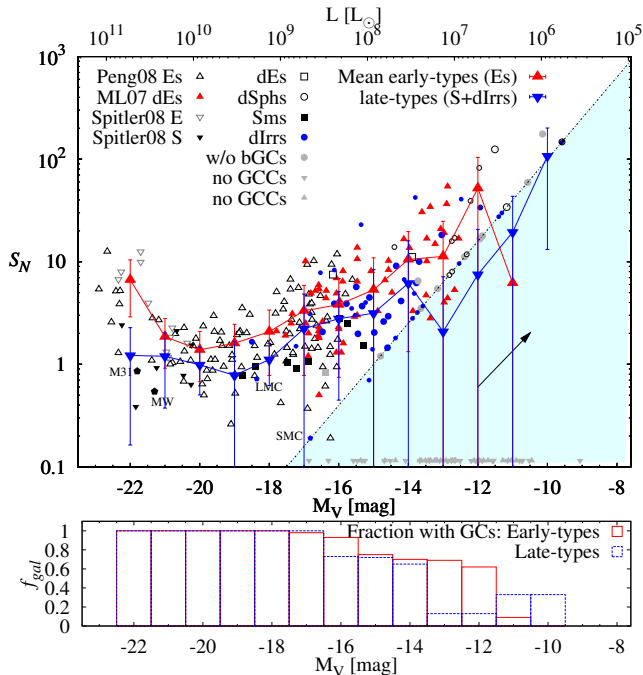


Figure 4. Top: GC specific frequency versus absolute galaxy magnitude for a range of galaxy masses, morphologies, and environments. The various symbol types are explained in the figure legend. Massive and dwarf elliptical galaxies as well as spirals have been collected from the literature as explained in Sect. 3.1. With larger symbol sizes (dots, circles and squares) we indicate the dwarf galaxies in our sample. Grey triangles at the bottom of the plot represent galaxies in which no GCCs were detected. The large symbols connected with a line are the co-added running average of the S_N values per magnitude bin for the different galaxy morphological types. The errorbars are the standard deviation at that magnitude bin. The dash-dotted line indicates the S_N value if a galaxy hosts one GC (cf. Eqn. 5). **Bottom:** Fraction of galaxies with GC detections for the magnitude bins used to derive the mean S_N value in the upper panel.

the Virgo galaxy cluster from Peng et al. (2008) and other massive elliptical and spiral galaxies from the compilation by Spitler et al. (2008) who selected galaxies with robustly derived GCS properties (deep photometry and completeness limits, adequate spatial coverage etc.) from the literature (Ashman & Zepf 1998; Rhode & Zepf 2001, 2003, 2004; Forbes et al. 2001; Forte et al. 2001; Dirsch et al. 2003, 2005; Gómez & Richtler 2004; Bassino et al. 2006b,a, 2008; Harris et al. 2006; Tamura et al. 2006a,b; Rhode et al. 2007). Our main source for the early-type dwarf galaxy data is Miller & Lotz (2007). For reference, we have labeled in Fig. 4 the corresponding S_N values of the Magellanic Clouds, M31, and the Milky Way. Keeping in mind the effects of passive evolutionary fading and star cluster disruption, the S_N vs. M_V trends for late- and early-type dwarfs in cluster and in loose environments appear very similar irrespective of galaxy morphological type and environment. With a dash-dotted line we indicate the lower limit of the S_N value defined by Equation 1 if the galaxy hosts one GC ($N_{GC} = 1$).

To investigate the S_N value as a function of galaxy morphology and luminosity we have estimated the mean S_N value in bins of one magnitude. With large open symbols connected with lines in Figure 4 we show these co-added

running averages of the S_N including galaxies without GC candidates. They have been computed by summing the number of GCs and galaxy luminosity for each magnitude bin. The error bars represent the standard deviation at that magnitude bin. It can be seen that late-type galaxies (spirals and irregulars) have on average (~ 2 times) lower mean S_N values at a given galaxy luminosity than early-type galaxies (ellipticals and spheroidals). This constant offset can be accounted for by evolutionary fading effects. The spiral galaxies in our sample show a fairly constant S_N value as a function of galaxy luminosity ($S_N \approx 1$). However, a larger sample increasing the number of spiral galaxies with luminosities $M_V < -19$ mag need to be studied to confirm the nearly constant S_N -value for spiral galaxies.

The bottom panel of Figure 4 shows an increasing fraction of galaxies with no detected old GCs towards decreasing galaxy luminosities. This decrease can be attributed to several factors affecting the galaxy luminosity normalized number of GCs: *i*) The increased impact of stochasticity for star-cluster formation and/or *ii*) the decrease of GC numbers due to dynamical destruction processes (i.e. evaporation, tidal disruption, etc.).

3.2 Specific Mass, Luminosity, and \hat{T} -value

In addition to the traditionally used specific frequency S_N , we discuss in the following the trends in the specific mass and specific luminosity of the GC system, as well as a redefined T -value (see Zepf & Ashman 1993) as a function of host galaxy luminosity and mass.

3.2.1 Specific Mass of GC system

We define the “specific mass” S_M as the total mass of the globular cluster system, \mathcal{M}_{GCS} , relative to the total baryon mass of the host galaxy defined as the sum of the stellar mass, \mathcal{M}_* , and the HI gas mass, \mathcal{M}_{HI} :

$$S_M = 100 \times \mathcal{M}_{GCS} / (\mathcal{M}_* + \mathcal{M}_{HI}). \quad (2)$$

This is similar to 100 times the McLaughlin (1999) ϵ parameter for the GC formation efficiency for giant galaxies with respect to the total baryon mass, which includes the mass of the hot, X-ray emitting halo. It is not a trivial task to include this mass component for the galaxies in our sample. Obtaining hot gas mass from X-ray profiles (M_X) relies on assumptions of the temperature profile as well as hydrostatic equilibrium, which is not always the case for galaxies in complex environments. For instance, the Fukazawa et al. (2006) X-ray observations of luminous early-type ellipticals in a range of environments show much weaker X-ray emission from isolated than for clustered galaxies. In addition, they find that the requirement for hydrostatic equilibrium might not be fulfilled for many of their ellipticals due to jets from AGNs and interaction with neighboring galaxies. In general, all cD galaxies in their sample (like NGC 1399) are classified as galaxies embedded in the hot cluster/group ISM. Therefore, the X-ray halo of such central cluster galaxies may have a non-negligible contribution from the galaxy cluster itself. To avoid problems with hydrostatic equilibrium Humphrey et al. (2006) and O’Sullivan et al. (2007) studied isolated elliptical galaxies for which they obtain M_X few times $10^8 M_\odot$,

a similar M_X mass was estimated for M 49 by McLaughlin (1999). Therefore, for the majority of the galaxies in our sample the expected M_X is of the order of few percent of the stellar mass, thus a negligible contribution to the total galaxy mass.

In the following we have considered the sum of the HI and stellar masses, $\mathcal{M}_* + \mathcal{M}_{HI}$, for the dwarf galaxies in our sample. Including the HI gas mass becomes more important when comparing massive elliptical galaxies with dwarf galaxies which can contain significant neutral gas mass fractions. The disadvantage of the S_M parameter (Eq. 2) is the necessary conversion from luminosity to mass, using \mathcal{M}/L ratio for the galaxy as well as the GCs (see below). On the other hand, S_M has the advantage of being a distance-independent quantity.

To derive \mathcal{M}_{GCS} for dIrrs we convert GC absolute magnitudes to masses using $\gamma_V \equiv (\mathcal{M}/L_V)_{GC} = 1.88$, which is the mean V -band mass-to-light ratio for old GCs in the LMC that we estimated from McLaughlin & van der Marel (2005). Since we are studying old globular clusters in similar galaxies, our choice of γ_V is justified and changes only within 10% for the age range of our GC sample selection ($t \gtrsim 4$ Gyr). However, a recent study by Kruijssen & Portegies Zwart (2009) showed that the GC \mathcal{M}/L ratio is expected to depend on cluster luminosity (mass) in that low-mass clusters preferentially lose low-mass, i.e. high \mathcal{M}/L , stars due to two-body relaxation. They show that this effect influences the translation from GC luminosity to mass function and the respective location of the turn-over mass (m_{TO}) toward lower mass by ~ 0.2 dex. This effect needs to be tested for a range of galaxy masses (i.e., tidal field strengths) in order to establish the GC $\mathcal{M}/L \propto L$ effect to the GCS m_{TO} . Keeping this in mind and assuming a constant GC \mathcal{M}/L for the GCSs of all galaxies, we will show in Sect. 4 that this effect is negligible relative to the observed spread/scatter in the relations that involve the GC \mathcal{M}/L ratio.

\mathcal{M}_{HI} was calculated from the HI magnitudes listed in the LEDA database (Paturel et al. 2003) or from HI fluxes in NED or Begum et al. (2008) following Roberts & Haynes (1994), i.e. $M_{HI} = 2.36 \times 10^5 \times D^2 \times F_{HI}$, where D is the distance in Mpc and F_{HI} is the HI flux in Jy km s^{-1} . To convert from galaxy luminosity to galaxy stellar mass \mathcal{M}_* , we used the relations in Bell et al. (2003) between the galaxy $B-V$ colour and the \mathcal{M}_*/L_V ratio (or $B-R$ if $B-V$ was not available):

$$\begin{aligned} \log(\mathcal{M}_*/L_V) &= -0.628 + 1.305 \times (B-V) \\ \log(\mathcal{M}_*/L_V) &= -0.633 + 0.816 \times (B-R). \end{aligned}$$

In addition to our dIrr galaxy data, we calculated \mathcal{M}_*/L_V ratios for elliptical and spiral galaxies from Peng et al. (2008); Spitler et al. (2008); Miller & Lotz (2007) and for dSphs and dIrrs from Sharina et al. (2005) and Seth et al. (2004) as follows. We use the stellar masses directly from the Peng et al. study which were computed from galaxy colours ($g-z$ and $J-K_s$). Spitler et al. (2008) used K -band photometry and theoretical \mathcal{M}_*/L_K from population synthesis models to derive galaxy mass, which we also adopt in the subsequent analysis. To derive baryonic masses for the dE sample in Miller & Lotz (2007) we use the galaxy magnitudes provided in their table and $\mathcal{M}_*/L_V = 3.0$. We used this mass-to-light ratio because the masses listed in their table were calculated assuming $\mathcal{M}_*/L_V = 5$ which seems

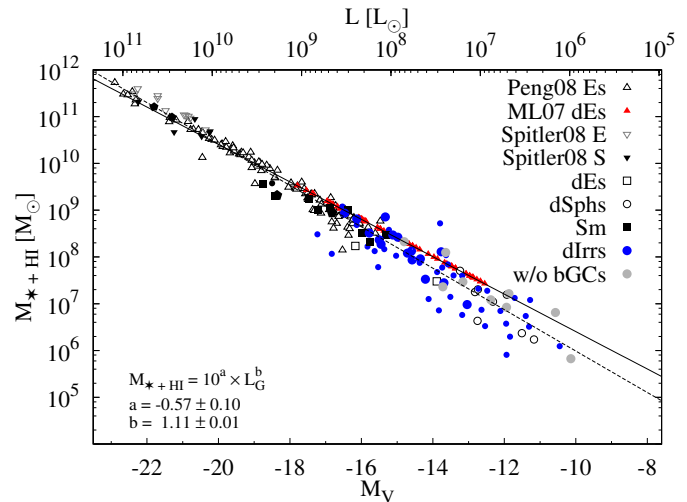


Figure 5. Stellar plus HI mass as a function of galaxy luminosity for dwarf galaxies in our sample (large solid dots) compared with galaxies of different morphological type from the literature as indicated in the legend. Smaller solid dots show dIrrs from Seth et al. (2004) and Sharina et al. (2005). With solid pentagons are shown (from left to right) M 31, Milky Way, LMC and SMC. The dashed line is a least-squares fit to the data; the fit relation and the values of the coefficients are given in the lower left corner. The solid line shows the relation between the galaxy luminosity and its mass with $\mathcal{M}_*/L_V = 3.0$.

to be too high and offset from the relation defined by our dataset and those of Seth et al. (2004); Sharina et al. (2005); Peng et al. (2008); Spitler et al. (2008) (see Fig. 5). For the dwarf galaxies in the Sharina et al. (2005) and Seth et al. (2004) samples we calculate their masses from the Bell et al. relations as we did for our sample. Note that uncertainties in the galaxy \mathcal{M}/L determination due to unknown SFHs and the choice of an IMF apply equally to the range of galaxy masses in our sample as to that of the SDSS and 2MASS galaxy samples from which the Bell et al. relations were derived.

In Figure 5 we illustrate the relation between galaxy luminosity and its stellar plus HI mass, \mathcal{M}_{*+HI} , for galaxies from the literature and the dwarf galaxies in our sample. We find an increasing difference with decreasing luminosity between the late-type, gas-rich, low-mass dIrrs, and early-type dwarf ellipticals, which are essentially devoid of HI. In addition, the low-mass dIrrs show an increasing dispersion towards fainter systems. This offset and dispersion can both be attributed to possibly underestimated \mathcal{M}_b/L_V due to younger stellar populations and/or unaccounted-for baryonic components in the form of, e.g. diffuse ionized gas, hot X-ray emitting gas, radio continuum emission or molecular gas. All these mass components are known to be associated with star formation activity and their mass fractions are observed to scale with galaxy HI mass (e.g. Dahlem et al. 2006).

3.2.2 Specific Luminosity of GC system

Another useful indicator of GC formation efficiency is the specific GC luminosity introduced by Harris (1991)

$$S_{L,V} = 100 \times L_{GCS}/L_V \quad (3)$$

which is the luminosity ratio between the GCS, L_{GCS} , and its host galaxy, L_V . Its main advantage as scaling parameter is that it is independent of distance and only weakly sensitive to completeness corrections at the faint end of the GC luminosity function (GCLF). A slight disadvantage of S_L is its sensitivity to the stellar population dominating the integrated light of the galaxy. For the case of late-type galaxies this typically is the most prominent (the latest) star formation episode, so that the galaxy luminosity does not necessarily indicate the stellar population at the time when most of the GCs were formed. On the other hand, S_L is independent of M/L and hence least affected by stellar population systematics. Thus, S_L may be the most robust GCS scaling parameter for comparing GCS richness and GC formation efficiencies between galaxies over large range of masses.

3.2.3 Modified T -value

Zepf & Ashman (1993) introduced the T value as the specific number of globular clusters per unit $10^9 M_\odot$ of the host galaxy mass, i.e. $T = 10^9 M_\odot \times N_{\text{GC}}/\mathcal{M}_*$. For our purposes this definition is insufficient since we want to compare gas-depleted early-type with late-type galaxies with significant gas mass fractions. Thus, we modify the T -value from Zepf & Ashman by including the gas mass of the host galaxy. Hence we define the specific number of GCs per unit baryonic mass $\hat{T}(\mathcal{M}_b)$ as follows:

$$\hat{T} = 10^9 M_\odot \times N_{\text{GC}}/\mathcal{M}_b \quad (4)$$

where $\mathcal{M}_b = \mathcal{M}_* + \mathcal{M}_{\text{HI}}$.

In Figure 6 we directly compare the GC specific frequencies (S_N , Eq. 1), the mass-normalized specific mass in clusters (S_M , Eq. 2), specific luminosities (S_L , Eq. 3), and the specific number (\hat{T} , Eq. 4) as a function of host galaxy luminosity for the entire sample.

4 DISCUSSION

In this section we address the question whether there is a physically motivated model which is able to describe the observed trends of the various scaling relations as a function of total galaxy mass. This can be tested by assuming that GCs form in proportion to the total galaxy mass. We start by comparing the GC scaling relations introduced in the previous Section 3 with theoretical model predictions that provide relations between the mass-to-light ratio and the total galaxy mass (Dekel & Silk 1986; Dekel & Birnboim 2006). The star-formation processes in these models are driven by (i) stellar feedback and (ii) shock heating below and above a critical stellar mass of $3 \times 10^{10} M_\odot$, respectively. Thus, we derive analytical expressions that can be used to confront the observed trends against the assumptions of constant and variable GC formation efficiencies as a function of galaxy luminosity. Observed differences and systematics can argue for or against physical mechanisms included (or the lack thereof) in the models we discuss.

Is the assumption of an universal mode of globular cluster formation among galaxies of different morphological type and environment justified? An universal GC formation scenario would predict that all (evolved) galaxies form their oldest star cluster populations with the same initial efficiency

at given galaxy mass. Subsequent formation of metal-rich GCs in massive galaxies would likely cause a spread in the observed GC formation efficiency value for a given range in galaxy mass since galaxies undergo different merging histories, varying from predominantly dissipational to mostly dissipationless. This can be tested by comparison of the expected value of the GC efficiency from the adopted analytical models and the observations of galaxies of the two major morphological types, early- versus late-types, and as a function of galaxy mass. The relative difference between the two galaxy types should be preserved at a given galaxy mass, assuming that GC destruction processes are similar to first order in both galaxy types.

In order to set quantitative constraints and limitations of the models we use, and address all questions discussed above, it is very important to normalize the model predictions, i.e. to put the models on an absolute scale. All studies, so far, which addressed the shape of the S_N distribution used one or another version of the Dekel & Birnboim models (e.g. Forbes 2005) but did not derive strict constraints due to the lack of such a normalization. Therefore, our effort in deriving a normalization will help to narrow down the possible physical processes that govern the spread in GC formation efficiencies among galaxies with similar mass. This is detailed in Section 4.2.1.

4.1 Boundaries of Globular Cluster Systems Scaling Relations

The definition of S_N (Eq. 1) determines the most trivial lower limit of star cluster population when $N_{\text{GC}} = 1$, i.e. the GC formation efficiency that resulted in only one old GC at present (and no additional field star component), so that

$$\log S_N = 6 + 0.4 M_V = 7.928 - \log L_V, \quad (5)$$

assuming $M_{V,\odot} = 4.82$ mag (Cox 2000). Analogously, we can derive similar relations for S_L , S_M and \hat{T} by assuming that the total luminosity and mass of the globular cluster system are $L_{\text{GCS}} = N_{\text{GC}} \times l_{\text{TO}}$ and $\mathcal{M}_{\text{GCS}} = N_{\text{GC}} \times m_{\text{TO}}$, where l_{TO} and m_{TO} are the cluster luminosity and cluster mass at the turn-over of the GCLF, respectively, hence

$$\begin{aligned} \log S_L &= 2 + \log l_{\text{TO}} - \log L_V \\ &= 2 + \log l_{\text{TO}} + 0.4 (M_V - M_{V,\odot}) \end{aligned} \quad (6)$$

$$\begin{aligned} \log S_M &= 2 + \log(m_{\text{TO}}/\Upsilon_V) - \log L_V \\ &= 2 + \log(m_{\text{TO}}/\Upsilon_V) + 0.4 (M_V - M_{V,\odot}), \end{aligned} \quad (7)$$

$$\begin{aligned} \log \hat{T} &= 9 - \log \Upsilon_V - \log L_V \\ &= 9 - \log \Upsilon_V + 0.4 (M_V - M_{V,\odot}) \end{aligned} \quad (8)$$

where $\Upsilon_V \equiv \mathcal{M}_*/L_V$ is the (overall) V -band stellar mass-to-light ratio of the host galaxy. The relations (5) to (8) are shown in Figure 6 with dash-dotted lines. For the derivation of S_M and \hat{T} we have adopted $\Upsilon_V = 3.0$, $l_{\text{TO}} = 8.47 \times 10^4 L_\odot$, and $m_{\text{TO}} = 1.69 \times 10^5 M_\odot$, which corresponds to $M_V = -7.5$ mag for $\gamma_V = 2.0$. Note that a change from $\Upsilon_V = 3.0$ to 1.0 and from $M_V = -7.5$ to -7.4 mag causes a parallel shift comparable to the symbol size relative to the relations.

Since the quantities S_N , S_L , S_M , and \hat{T} involve properties of GC systems that are (often) measured down to the turnover luminosity of the GC luminosity function, it is useful to assess the uncertainties associated with Eqs. 5 – 8. The results of Jordán et al. (2007) show that the dispersion (σ) and turn-over luminosity (l_{TO}) of the GCLF changes as a function of host galaxy luminosity. The same study shows also that the mass at the GCLF turnover is roughly constant (see also Vesperini 1998, 2000) and decreases by $\sim 30\%$ from $m_{\text{TO}} = (2.2 \pm 0.4) \times 10^5 M_\odot$ in the brightest galaxies down to $m_{\text{TO}} \simeq (1.6 - 1.7) \times 10^5 M_\odot$ in dwarf elliptical galaxies, with a substantial scatter in the latter. For comparison, in our analysis of the GCLF in mainly late-type dwarf galaxies we derive a GCLF turnover mass $m_{\text{TO}} = 1.6 \times 10^5 M_\odot$ (Georgiev et al. 2008) assuming $\gamma_V = 1.88$, which is the mean value of the mass-to-light ratio of old GCs in the LMC and SMC dIrrs (McLaughlin & van der Marel 2005). Due to the fact that the HST/ACS field of view entirely covers the dwarf galaxies in our sample we observe the total GC population and derive an accurate *total* S_N^4 . Doing so we find that the predictions of the Equations (5) to (8) are accurate to within $\sim 30\%$ for our sample of late-type dwarf galaxies.

The above relations can be understood as a minimum GC formation efficiency threshold. In other words, the inverse scaling relations with galaxy L_V suggest that dwarf galaxies at fainter total luminosities are either more efficient in forming star clusters relative to the formation of field stars or less efficient in the formation of field stars than more luminous systems (see Fig. 6). We have discussed above (see Sect. 3.1) that passive luminosity fading of the host is almost parallel to this lower limit and leads to an increase in the S_N value, provided the GC population size remains constant. However, it should be noted that the slope observed in the data partially reflects the slope stemming from the definition of these equations.

4.2 Globular Cluster System Scaling Relations as a Function of Galaxy Mass

All panels in Figure 6 strengthen the previously observed increasing GC formation efficiency with decreasing galaxy luminosity for galaxies fainter than $M_V \approx -20$ mag. This trend is preserved even when the GC number (or mass) is compared to the *total* host galaxy mass. Theoretical models of star-formation processes regulated by supernova feedback in low-mass halos (e.g. Dekel & Silk 1986; Dekel & Woo 2003), predict an increasing total \mathcal{M}_h/L with decreasing halo mass. The assumption that the number of GCs could be a function of host galaxy mass-to-light ratio and environmental density have been investigated in previous studies of early-type galaxies (e.g. Forbes 2005; Bekki et al. 2006; Peng et al. 2008, and references therein).

In the following we derive analytical expressions which relate the observed *specific formation efficiency* of old GCs in galaxies as a function of *total* halo mass \mathcal{M}_h . Under the assumption that GCs form in proportion to the mass of the

host galaxy, i.e. the total GC system mass \mathcal{M}_{GCS} is directly related to \mathcal{M}_h as:

$$\mathcal{M}_{\text{GCS}} \equiv \eta \mathcal{M}_h, \quad (9)$$

where η represents an empirical formation efficiency parameter, which is the *specific globular cluster formation efficiency*. This parameter describes the total observed mass fraction in globular clusters, which is a product of the initial cluster formation efficiency (initial cluster mass function) and various mechanisms of cluster dissolution (e.g. two-body relaxation, GMC encounters, tidal shocking and dynamical friction). Note that our sample dwarf galaxies have old GCs with ages expected from their $V - I$ colour of $t \gtrsim 4$ Gyr, hence, we are probing the early, post-violent relaxation phases of GC formation and their dissolution history with respect the field stellar population. In the following, we assume that the total GC system mass and its corresponding total luminosity are related through

$$L_{\text{GCS}} = \mathcal{M}_{\text{GCS}}/\gamma_V \quad (10)$$

where γ_V is the mean V -band GC mass-to-light ratio.

The observed GC system scaling relations have been tied by previous studies (e.g. Forbes 2005) into the galaxy formation context using the models of Dekel & Silk (1986) according to which star formation in dark-matter halos below a stellar mass of $\mathcal{M} \approx 3 \times 10^{10} M_\odot$ ($\mathcal{M}_h \sim 10^{12} M_\odot$) is governed by the thermal properties of the inflowing gas which are primarily regulated by supernova (SN) feedback. These models predict that the mass-to-light ratio evolution of mini-halos follows $\mathcal{M}_h/L_V \propto \mathcal{M}_h^{-2/3}$ (Dekel & Woo 2003), so that $L_V \propto \mathcal{M}_h^{5/3}$.

The latest models on star formation regulated by shock-heating (Dekel & Birnboim 2006) predict that above this characteristic stellar mass ($\mathcal{M} \approx 3 \times 10^{10} M_\odot$), the gas inflow experiences a virial shock (“hot stream”) and, hence, is more susceptible to feedback leading to suppressing star formation. This physical transition leads to a different mass-to-light ratio scaling that follows $\mathcal{M}_h/L_V \propto \mathcal{M}_h^{1/2}$ or $L_V \propto \mathcal{M}_h^{1/2}$ for $\mathcal{M} \gtrsim 3 \times 10^{10} M_\odot$.

4.2.1 Normalization of the Scaling Relations

In order to obtain a *quantitative* description of the specific GC formation efficiency as a function of galaxy halo mass we must normalize these scaling relations. We, therefore, assume the following normalization relations

$$\kappa_1 L_V = \mathcal{M}_h^{5/3} \quad \text{for } \mathcal{M} < 3 \times 10^{10} M_\odot \quad (11)$$

$$\kappa_2 L_V = \mathcal{M}_h^{1/2} \quad \text{for } \mathcal{M} > 3 \times 10^{10} M_\odot. \quad (12)$$

Such a normalization has not been investigated by previous studies (e.g. Forbes 2005). To empirically calibrate the model predictions in the low-mass, SN-feedback regulated star formation regime ($\mathcal{M} < 3 \times 10^{10} M_\odot$), we use the results from Strigari et al. (2008) who measure dynamical masses within the inner 0.3 kpc of many Local Group dwarf galaxies over a wide range of luminosities ($10^3 - 10^7 L_\odot$). Strigari et al. find that all dwarfs have a “universal” central mass of $\mathcal{M}_{0.3\text{kpc}} = 10^7 M_\odot$. This central dynamical mass can be tied through high-resolution cold dark matter (CDM) simulations to the total halo mass via $\mathcal{M}_h \simeq \mathcal{M}_{0.3\text{kpc}}^{1/0.35} \times 10^{-11} M_\odot$, based on the models of Bullock et al. (2001). Below the

⁴ Note that the original definition of Harris & van den Bergh (1981) is to double the number of GCs brighter than the GCLF turnover luminosity to obtain N_{GC} in Equation 1. This is identical to the total N_{GC} only if the GCLF is symmetric

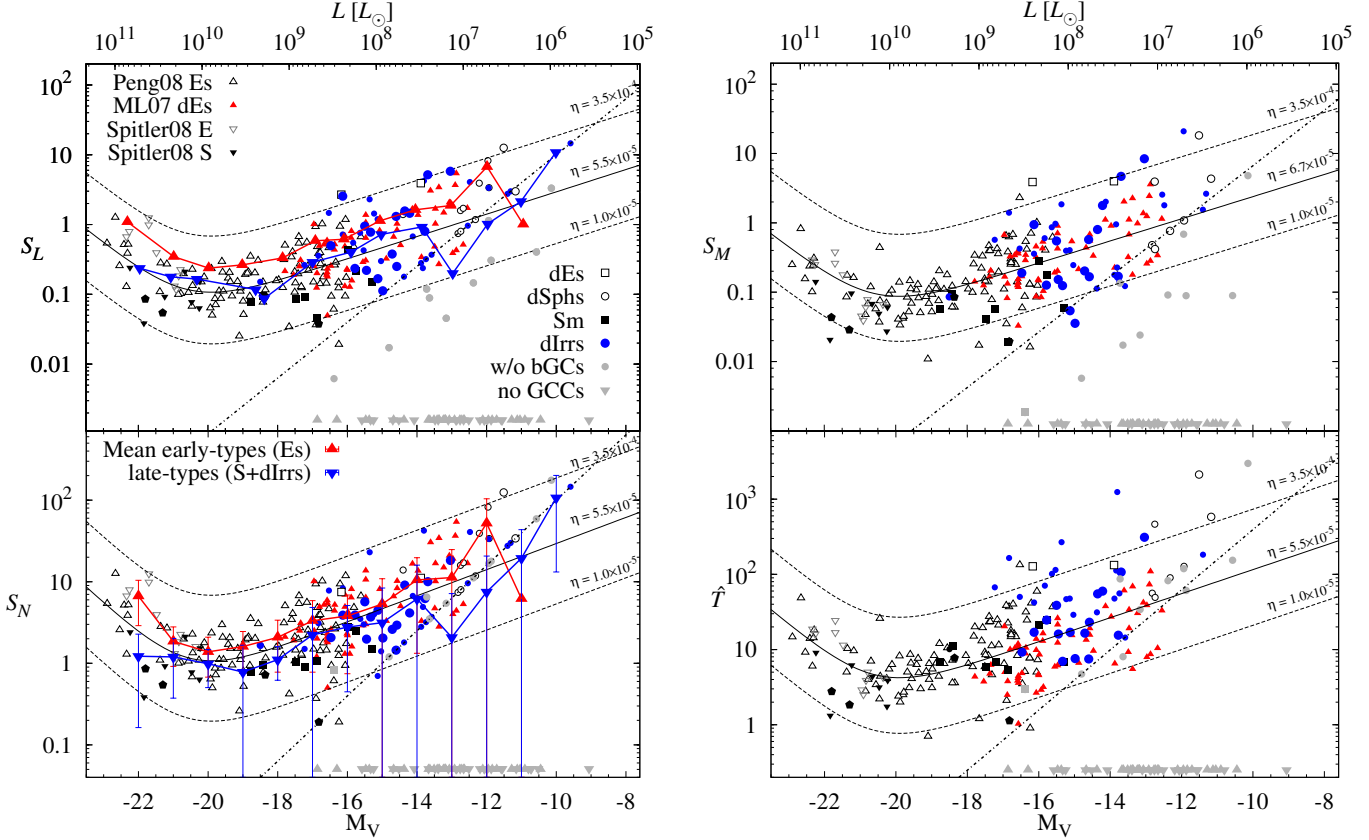


Figure 6. Globular cluster system scaling parameters as a function of galaxy luminosity. From top left to bottom right are shown the GC specific specific luminosities (S_L), specific mass (S_M), specific frequencies (S_N), and specific number (\hat{T}) for all galaxies in the combined sample. Large solid dots indicate dIrrs from our study, while small solid dots are dIrrs from Seth et al. (2004); Sharina et al. (2005) and Georgiev et al. (2006). Solid pentagons show the corresponding values for the Milky Way, M31, LMC and SMC. Grey triangles show galaxies in which no GC candidates are detected. The dash-dotted line represents the corresponding value if galaxy hosts one GC at present, see Sect. 4.1. The solid curves are predictions by the models which assumes that GCs form proportional to the total galaxy halo mass and that stellar, SNe-driven feedback and virial shock-heating regulate galaxy wide star formation (Dekel & Birnboim 2006), below and above $\mathcal{M} \simeq 3 \times 10^{10} M_\odot$, respectively (see Sect. 4.2). The solid curve (top panels) is the best-fit $\eta_L = 5.5$ and $\eta_M = 6.7 \times 10^{-5}$ value to the S_L and S_M distributions, respectively. The solid lines in the bottom panels are curves with adopted $\eta_L = 5.5 \times 10^{-5}$. Large triangles connected with solid lines in the left panels show the co-added running average S_N and S_L values as a function of galaxy luminosity for early- and late-type systems. Dashed curves illustrate the range in η values among galaxies, between $\eta = 10^{-5}$ to 3.5×10^{-4} .

critical mass of $\mathcal{M} = 3 \times 10^{10} M_\odot$ this leads to $\kappa_1 = (\mathcal{M}_{0.3\text{kpc}}^{1/0.35} \times 10^{-11})^{5/3} / L_V$. For L_V , we choose $L_V = 10^6 L_\odot$ as the lowest luminosity of a stellar system that can possibly form one GC. Furthermore, the dynamical mass measurements of Strigari et al. are less dominated by observational errors at this luminosity. For the high-mass, “virial-shock” regime we base the determination of κ_2 on empirical results for the virial mass to B -band light ratio at $3 \times 10^{10} M_\odot$: $\mathcal{M}_{\text{vir}}/L_B = 75$ from Eke et al. (2006) based on galaxy group dynamics. From SSP models at solar metallicity (Bruzual & Charlot 2003) we derive $(\mathcal{M}/L_B)/(\mathcal{M}/L_V) = 1.65$ at 14 Gyr which leads to $\mathcal{M}_{\text{vir}}/L_V = 41$. Hence, we obtain $L_V = 6.67 \times 10^8 M_\odot$, i.e., $\kappa_2 = 10^{-4.42}$ for the high-mass regime. Thus, we have

$$10^9 L_V = \mathcal{M}_h^{5/3} \quad \text{for } \mathcal{M} < 3 \times 10^{10} M_\odot \quad (13)$$

$$10^{-4.42} L_V = \mathcal{M}_h^{1/2} \quad \text{for } \mathcal{M} > 3 \times 10^{10} M_\odot. \quad (14)$$

Using Equations (9) through (11) we can express the scaling relation defined by Equations (1), (2), (3), and (4) as a

function of galaxy absolute magnitude for the “SN feedback” regime at stellar mass $\mathcal{M}_h < 3 \times 10^{10} M_\odot$:

$$\log S_N \simeq 6 + 0.24 \times M_{V,\odot} + \log \left(\frac{\eta \kappa_1^{0.6}}{m_{\text{TO}}} \right) + 0.16 M_V \quad (15)$$

$$\log S_L \simeq 2 - 0.16 \times M_{V,\odot} + \log \left(\frac{\eta \kappa_1^{0.6}}{\gamma_V} \right) + 0.16 M_V \quad (16)$$

$$\log S_M \simeq 2 - 0.16 \times M_{V,\odot} + \log \left(\frac{\eta \kappa_1^{0.6}}{\Upsilon_V} \right) + 0.16 M_V \quad (17)$$

$$\log \hat{T} \simeq 9 - 0.16 \times M_{V,\odot} + \log \left(\frac{\eta \kappa_1^{0.6}}{m_{\text{TO}} \Upsilon_V} \right) + 0.16 M_V \quad (18)$$

where Υ_V is the baryonic V -band mass-to-light ratio of the host galaxy, m_{TO} is the GCLF turn-over GC mass, and γ_V is the corresponding GC mass-to-light ratio. The scaling relations as a function of galaxy luminosity L_V , total halo mass \mathcal{M}_h , and baryonic mass \mathcal{M}_b are given in Appendix A.

For the “virial shock” regime at masses $\mathcal{M} > 3 \times 10^{10} M_\odot$ ($\mathcal{M}_h \gtrsim 10^{12} M_\odot$) the above scaling relations have the following functional forms:

$$\log S_N \simeq 6 + 0.8 \times M_{V,\odot} + \log \left(\frac{\eta \kappa_2^2}{m_{\text{TO}}} \right) - 0.4M_V \quad (19)$$

$$\log S_L \simeq 2 + 0.4 \times M_{V,\odot} + \log \left(\frac{\eta \kappa_2^2}{\gamma_V} \right) - 0.4M_V \quad (20)$$

$$\log S_M \simeq 2 + 0.4 \times M_{V,\odot} + \log \left(\frac{\eta \kappa_2^2}{\Upsilon_V} \right) - 0.4M_V \quad (21)$$

$$\log \hat{T} \simeq 9 + 0.4 \times M_{V,\odot} + \log \left(\frac{\eta \kappa_2^2}{m_{\text{TO}} \Upsilon_V} \right) - 0.4M_V. \quad (22)$$

4.2.2 Continuous description of the GCS scaling relations

In order to simultaneously describe the observed trends in the various GCS scaling relations in the stellar/SNe-dominated feedback regime *and* the regime where star-formation is primarily regulated by virial shock-heating of the inflowing gas, we combine the above sets of relations above and below the characteristic galaxy stellar mass at $\mathcal{M} \sim 3 \times 10^{10} \mathcal{M}_\odot$:

$$S_N = \frac{\eta 10^6}{m_{\text{TO}}} \left(\kappa_1^{0.6} 10^{0.16M_V + 0.24M_{V,\odot}} + \kappa_2^2 10^{-0.4M_V + 0.8M_{V,\odot}} \right) \quad (23)$$

$$S_L = \frac{\eta 10^2}{\gamma_V} \left(\kappa_1^{0.6} 10^{0.16(M_V - M_{V,\odot})} + \kappa_2^2 10^{-0.4(M_V - M_{V,\odot})} \right) \quad (24)$$

$$S_M = \frac{\eta 10^2}{\Upsilon_V} \left(\kappa_1^{0.6} 10^{0.16(M_V - M_{V,\odot})} + \kappa_2^2 10^{-0.4(M_V - M_{V,\odot})} \right) \quad (25)$$

$$\hat{T} = \frac{\eta 10^9}{m_{\text{TO}} \Upsilon_V} \left(\kappa_1^{0.6} 10^{0.16(M_V - M_{V,\odot})} + \kappa_2^2 10^{-0.4(M_V - M_{V,\odot})} \right) \quad (26)$$

Solid and dotted curves in Figure 6 illustrate the relations from Eqs. (23) to (26), for various values of η . It can be seen that these scaling relations approximate the observed distributions fairly well and indicate a statistically significant spread in the mass and luminosity normalized GC formation efficiencies η_L and η_M (top panels in Fig. 6). The co-added running average S_L and S_N values as a function of galaxy luminosity for early- and late-type systems (connected with solid line large triangles in the left panels of Fig. 6) also show that they compare well with the analytical model expectation.

The remarkably good description of the observations by the analytical model advocates that at low galaxy masses, where galaxies have shallower potential wells (i.e., lower binding energy), gas is effectively heated up by the ionizing radiation of SNe suppressing star-formation. In the view of the Dekel & Birnboim models star-formation in massive and dense molecular clouds is effectively shielded from heating radiation which does not significantly influence cluster formation but suppresses more effectively the formation of field stars which leads to an increase in the GCS scaling parameters. Thus, at low-galaxy masses the initial burst of star formation leads to the formation of the old metal-poor GCs. The subsequent cooling of the galaxy ISM and its chemical enrichment can lead to the formation of metal-rich and younger GCs triggered by instability of internal (tidal density waves and/or collisions of stellar winds) or external (e.g. galaxy-galaxy interaction) origin. Examples are the metal-rich ($[\text{Fe}/\text{H}] \lesssim -0.5$) and young ($> \text{few Gyr}$) clusters in the Magellanic Clouds and Local Group (LG) dwarf galaxies.

This is consistent with the recent age-metallicity relation (AMR) derived for those systems (Forbes & Bridges 2010; Sharina et al. 2010). These studies show that the formation of star clusters in low-mass systems captures a snapshot of the enrichment history of the host galaxy which is a function of host mass expressed by the metallicity-luminosity relation of dSphs/dIrr galaxies (e.g. Mateo 1998; Crnojević et al. 2010; Lianou et al. 2010). If some of the red GCs in our sample are indeed young (see discussion in Sect. 3.1.1) this might support this scenario.

With increasing galaxy mass, the galaxy potential deepens, the binding energy is larger, which leads to a more effective field star-formation efficiency at the same initial GC formation efficiency, thus causing the decrease in scaling parameters, e.g. S_L . Beyond the virial shock-heating galaxy mass, dense molecular clouds are better shielded than the lower-mass, less compact gas clouds in which most of the field star-formation will occur. On the one hand, this will lead to a nearly universal initial GC formation efficiency, on the other hand, to a more efficiently suppressed field star-formation efficiency. This will cause the observed upturn in S_L at high galaxy masses. That is, at the transitional stellar mass of $\mathcal{M} \sim 3 \times 10^{10} \mathcal{M}_\odot$ the thermal properties of the inflowing gas are primarily governed by virial shocks which heat the ISM and inhibit the efficient formation of field stars at the same initial GC formation efficiency. The variance between the observed and expected S_L values for this model can be in part explained by the interplay of dissipational and dissipationless galaxy merging. Observations support the formation of more and metal-rich clusters during gas-rich mergers (e.g. Whitmore & Schweizer 1995; Whitmore et al. 1999; Goudfrooij et al. 2007). Semi-analytical models of cluster formation are able to reproduce the GC metallicity and age distributions assuming formation of GCs during galaxy merging (e.g. Muratov & Gnedin 2010).

4.3 The Distribution of Globular Cluster Formation Efficiencies

In the following we investigate the specific GC formation efficiency η as a function of galaxy luminosity and morphology. To derive the distribution of η we choose S_M and S_L (upper panels in Fig. 6) as their values are least affected by internal systematics. Both parameters are independent of distance and are nearly insensitive to incompleteness of low-mass, faint GCs (see Sect. 3.2 and also Harris 1991, 2001). This is reflected in a smaller observed scatter in S_M and S_L values around the best-fit iso- η relation compared to the S_N and \hat{T} values. The advantage of the S_M value is that variations in stellar population parameters of the host galaxies and GC systems (i.e., their star-formation histories) are taken into account by the galaxy M/L (see Sect. 3.2). However, we point out that the derived Υ_V for low-mass dwarf irregular galaxies, which is based on galaxy colours, is likely to have an increased uncertainty due to their likely different SFHs relative to the sample of more massive galaxies from which the Bell et al. relations were derived (2MASS & SDSS galaxies). We invert Equations (24) and (25) to derive η values for our sample galaxies. The resulting η distributions as a function of galaxy luminosity are shown in Figure 7. To test for trends of the GC formation efficiency as a function of galaxy luminosity and morphology we formed the running

average for η_L and η_M as a function of galaxy luminosity in galaxy luminosity bins of $M_V = 1$ mag, same as in Figure 4. The mean values are shown with solid curves and different symbols for the two galaxy morphology classes. The errors in the running average, not shown for clarity purposes, correspond to approximately ${}^{+1.0}_{-1.5}$ dex.

The direct comparison between the η_L and η_M distributions in Figure 7 shows good agreement for early-type galaxies which indicates a robust understanding of their mass-to-light ratios. However, for late-type galaxies the systematically lower $\bar{\eta}_M$ with decreasing galaxy luminosity is caused by dwarfs without GC candidates. Those GC-free dwarf galaxies contribute mostly stellar light/mass but no GCs, i.e. the normalized GC formation efficiency is reduced at a given galaxy magnitude bin.

Assuming consistent $\bar{\eta}_M$ and $\bar{\eta}_L$ distributions for dIrrs this translates into various (degenerate) systematics that are not included in the models, namely *i*) a growing mass component towards fainter galaxy luminosities, *ii*) a steeper IMF in low- L dIrr galaxies, or/and *iii*) a systematically higher internal extinction value in low-mass galaxies. The investigation of these systematics suggests a mass-dependent term $\alpha(\mathcal{M}_h)$ in the scaling relation $\mathcal{M}_h/L_V \propto \mathcal{M}_h^{-2/3+\alpha(\mathcal{M}_h)}$ that is currently unaccounted for in the Dekel & Birnboim models. The quantification of such a term goes beyond the scope of this paper and requires much more comprehensive GCS samples across the entire range of late-type galaxies from low-mass dwarf irregulars to massive spirals.

The fits to the $S_L - M_V$ and $S_M - M_V$ distributions return $\langle \eta_L \rangle = 5.5 \times 10^{-5}$ and $\langle \eta_M \rangle = 6.7 \times 10^{-5}$ for the luminosity- and mass-normalized GC formation efficiencies, respectively. Those are shown with solid curves in the top panels in Figure 6. Because of the uncertainty in the derived galactic Υ_V affecting η_M we adopted the $\eta_L = 5.5 \times 10^{-5}$ for the bottom panels in Figure 6. The data can be approximated by a wide range of specific GC formation efficiencies from $\eta \simeq 10^{-5}$ to $\simeq 5 \times 10^{-4}$. The varying scatter in η_L as a function of galaxy luminosity is at least partly due to the increasingly stochastic nature of star and star-cluster formation processes towards lower galaxy masses. This is supported by the observational errors which are lower at higher galaxy luminosities (cf. Fig. 2) which relate to smaller standard deviations of η_L (cf. top left panel of Fig. 7). At the faintest galaxy luminosities the η_L distribution is affected by the minimum- η_L relation (discussed in Sect. 4.1) which narrows its distribution. The large scatter in η_M at faint galaxy luminosities (relative to that of η_L) is primarily driven by the poor knowledge of the galaxy's \mathcal{M}/L -ratios based on optical colours.

The value of the mean GC formation efficiency, η , that we obtain is consistent with previous estimates by Blakeslee (1999); McLaughlin (1999); Kravtsov & Gnedin (2005); Spitler & Forbes (2009). The value of $\eta_b = 1.71 \times 10^{-4}$ obtained by Blakeslee (1999) is the GC formation efficiencies with respect the baryon galaxy mass (stellar plus hot gas mass) derived for massive elliptical galaxies. Multiplying this value by $f_b = 0.17$, the universal cosmological baryon fraction observed by WMAP (Hinshaw et al. 2009), leads to $\eta_h = 2.9 \times 10^{-5}$. This value is identical to the η -values obtained by us, Kravtsov & Gnedin (2005) and Spitler & Forbes (2009), $\eta_h = 2 - 5 \times 10^{-5}$ and 7.1×10^{-5} , respectively.

To investigate how η relates to different galaxy morphologies we show histogram distributions in Figure 8 for the different morphological types: dIrrs, dSphs, dEs, spirals, and ellipticals. For those samples we derive the highest probability density distributions excluding the dwarfs with no blue or any GC detection (discussed in Fig. 7). The number of such galaxies in the dIrrs, dSphs, dEs, Es and spirals samples, respectively, is: 44 (51%), 4 (60%), 16 (18%), 0 and 3 (15%). For η_L , we find no evidence for a statistically significant offset in the average values $\langle \eta_L \rangle$ between late-type and early-type galaxies (see legend in Fig. 8) even though the scatter around the average value is larger for the fainter dwarf galaxies as mentioned above. We do however find a marginally significant offset between the $\langle \eta_L \rangle$ values of dIrrs and dEs. The fact that this offset is larger for $\langle \eta_M \rangle$ than for $\langle \eta_L \rangle$ suggests that it is mainly due to a systematic difference in stellar population properties between dIrrs and dEs.

In general, an offset in η_L versus η_M between late- and early-type galaxies can be expected due to a difference in stellar population parameters of GCs and their host galaxies. An increase in γ_V by $\sim 10\%$, which corresponds to a few Gyr age difference within the age range of our sample selection ($t_{GC} \gtrsim 4$ Gyr), introduces a shift in the η_L distribution towards larger values ($\Delta \log \eta_L = 0.03$), which is insufficient to account for the observed difference in η . However, luminosity fading of the host galaxy of the order of $\Delta M_V = 1.0$ to 1.5 mag (see Sect. 3.1) would cause $\log \eta_L$ to shift by 0.24 to 0.36 dex towards higher values, which would be enough to equalize the η_L distributions of late-type and early-type galaxies. Although some of our sample dIrrs may require such luminosity corrections (in particular those with very low η_L), most of our sample dIrrs lack any evidence for significant present-day star formation rates which suggests that evolutionary fading corrections of their galaxy light might not be required. On the other hand, the mass-normalized GC formation efficiency η_M should in principle correct for any stellar population age difference between late- and early-type galaxies. What we observe instead in Figure 8 is that the late-type galaxies in our sample (dIrrs and spirals) have lower average η_M than the early-type galaxies at the same luminosity, suggesting that the \mathcal{M}/L -ratios of the late-type galaxies may be underestimated (as already discussed above in the context of Fig. 7). However, the number of spiral galaxies in our sample is only marginally significant to draw statistically meaningful conclusions. Therefore, a more comprehensive study including near-infrared imaging or spectroscopic observations (lacking for the majority of the dwarfs in our sample) should help in resolving this issue.

Finally, we note that the minimum η -limit described by Eq. (5) intercepts the iso- η line for the maximum observed specific GC formation efficiency (Eq. 24) at $M_V \approx -9$ mag, corresponding to $3.37 \times 10^5 L_\odot$ (cf. Fig. 6). In the context of our assumptions, this magnitude describes the lowest luminosity halo that, on average, can form and host one old GC. This is consistent with the fact that the recently found extremely faint Local Group dwarf galaxies do not possess GCs (e.g. Belokurov et al. 2006, 2007; Irwin et al. 2007; Walsh et al. 2007; Willman et al. 2005a,b; Zucker et al. 2006a,b).

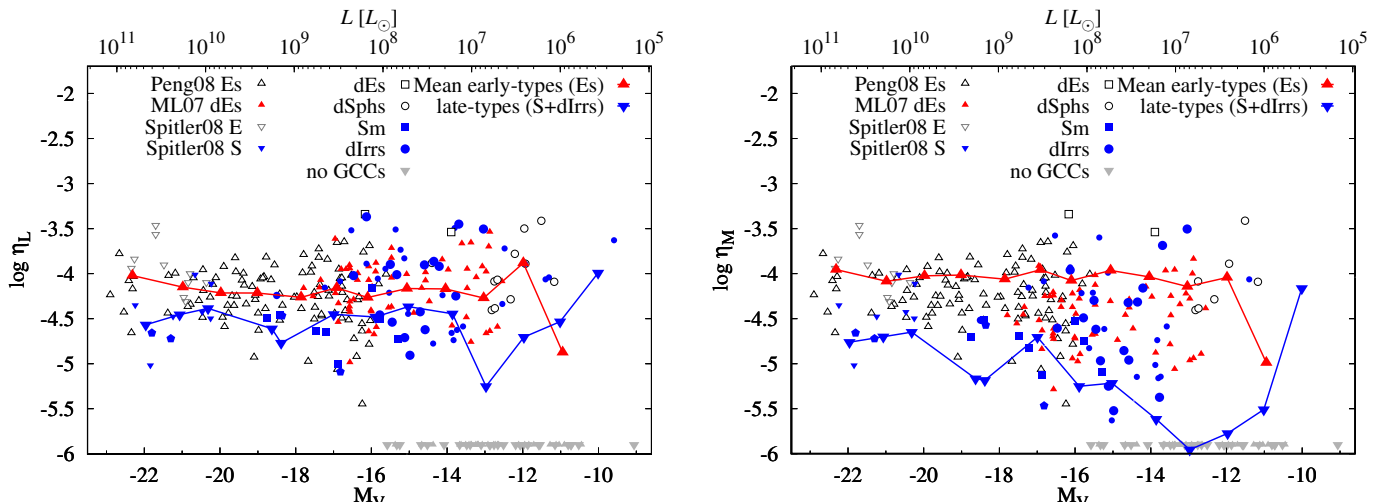


Figure 7. Specific globular cluster formation efficiencies, η , as a function of galaxy luminosity. **Left:** Luminosity normalized GC formation efficiency (η_L) derived from the S_L relation (eqn. 24). **Right:** Mass normalized GC formation efficiency (η_M) derived from the S_M relation (eqn. 24). The symbols connected with lines show the mean η values (including galaxies without GCCs) in bins of one magnitude. The remaining symbols are as in Figure 6.

4.4 Implications for Hierarchical Galaxy Formation

4.4.1 The Influence of various Physical Processes on the Variance of Globular Cluster Formation Efficiencies

The general behavior of the GC system scaling relations implies that the star and star-cluster formation processes scale with the total host galaxy mass. However, it is not yet clear what is driving the large observed galaxy-to-galaxy scatter in the η values for galaxies with otherwise similar mass. Environmental density is one of the suggested parameters to cause systematic trends in this regard (Peng et al. 2008). The majority of our current dIrr galaxy sample consists of *field* dIrrs, with a dearth of dIrrs situated in *cluster* environments. Conversely, dE galaxies with GC data available in our literature compilation are all located in the Virgo cluster Miller & Lotz (2007); Peng et al. (2008). Hence we cannot yet make a statistically significant comparison between the GC formation efficiency of field and cluster dwarf galaxies. To robustly assess the impact of environmental density on the η distribution will require the investigation of more dIrr galaxies in dense groups and galaxy clusters and more dE galaxies in loose environments.

Another explanation for the scatter in η can be obtained from the different timing of star cluster vs. field star formation as a function of the star formation rate of the host galaxy. For the latter, Larsen & Richtler (2000) demonstrated that the specific U -band luminosity in young massive star clusters in late-type galaxies strongly correlates with the total star formation rate and star formation rate surface density of the host galaxy, SFR and Σ_{SFR} , respectively. Thus, galaxies with the same mass but different SFR histories will have different GC formation efficiencies, since galaxies with higher peak SFRs will produce larger numbers of massive GCs that will survive a Hubble time.

Furthermore, a delay between the peak formation epochs of star clusters and field stars that scales with SFR (in the sense that the star clusters form earlier on average than the field stellar population) will increase the values of the GC system scaling parameters, especially for more vio-

lent starbursts which likely form more star *clusters* per unit gas mass. Any truncation of star-formation processes before the formation of the field stellar population is complete (e.g., through gas stripping during infall into a dense galaxy cluster medium) would further increase the GC scaling parameters. A hint that such effects might be at work was provided by Peng et al. (2008) who correlated the SFR and Σ_{SFR} with the mass fraction of GCs in their sample galaxies to find that the cluster formation rate peaks ~ 500 Myr earlier than the total galaxy SFR.

Another plausible mechanism to account for an apparent variation in η among galaxies is GC stripping and accretion (Côté et al. 1998, 2002; Hilker et al. 1999) that can cause a steeper slope of the $S_L - M_V$ relation at brighter galaxy luminosities, where the accretion of high- η dwarf galaxies may be an important mechanism during the early epochs of massive galaxy assembly. Such dwarfs may have completed the process of star-cluster formation at high redshifts ($z \gg 2$) and had their field star-formation processes suppressed or stopped (due to shock heating) during their infall through the dense intracluster medium.

4.4.2 Predictions from a Simplistic Accretion Model

Some of the most luminous early-type galaxies in our sample show excess η values ($\log \eta \approx -3.5$) that may indicate that their GCSs either experienced an early, highly-efficient episode of massive cluster formation followed by a shutoff of (field) star formation or that their GCSs were supplemented with high- η low-mass dwarf galaxies and their GC systems (or a combination of both effects). Such low-mass dwarfs would mainly contribute to the blue GC population and rather less to the field stellar component, and could well account for the observed high ratio of the metal-poor GCs to metal-poor field (halo) stars in massive galaxies (e.g., Harris & Harris 2002). Côté et al. (1998) and Hilker et al. (1999) suggested that faint ($M_V \approx -12$ mag) dwarfs accreted by cD galaxies can indeed provide the right number of GCs to account for their high S_N . We can make a simple estimate of the number and luminosity of satellite galaxies necessary

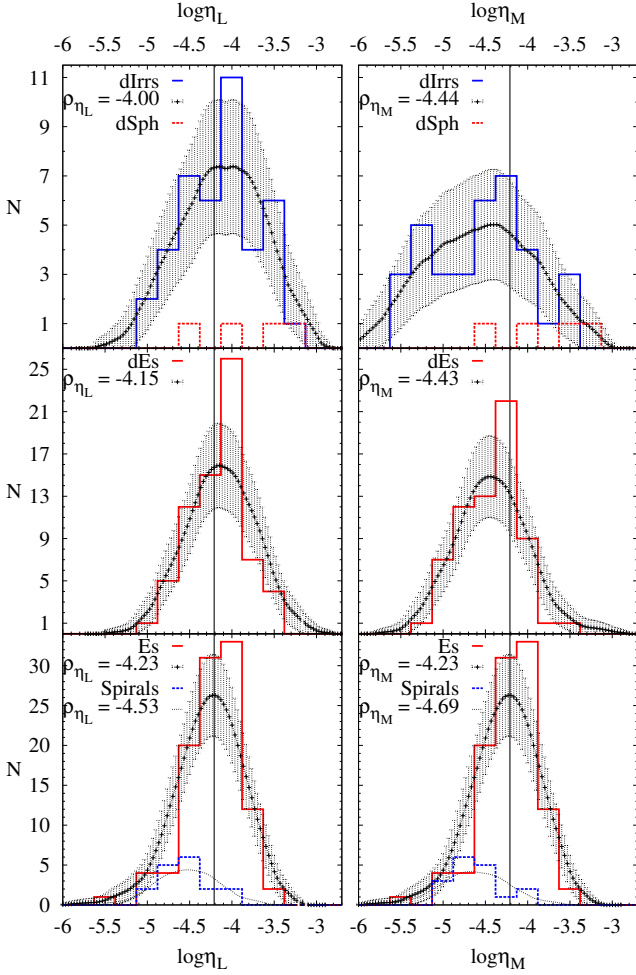


Figure 8. Specific GC formation efficiency, η , for various galaxy types: dIrr, dSph, dE, elliptical and spiral galaxies (top to bottom panels). *Left panels:* luminosity normalized GC formation efficiency (η_L) distributions. Those for dIrrs are *not* corrected for evolutionary fading of the integrated galaxy light. *Right panels:* mass normalized GC formation efficiency (η_M) distributions. Dashed-dotted curves with Poisson errors are Epanechnikov-kernel probability density estimates. The maximum-likelihood η values for the different galaxy samples are shown in the upper left corner of each panel. The vertical solid line in all panels shows for comparison the η -value for Es. Fading of $\Delta M_V = 1.5 - 1$ mag will shift the log η distribution of late-types toward higher values by $0.36 - 0.24$ dex.

to increase the S_L value of a progenitor galaxy by a certain value by simply using the definition of S_L (Eq. 3):

$$S_L = 10^2 \frac{L_{GCS,prg} + N_{acc} \times L_{GCS,acc}}{L_{V,prg} + N_{acc} \times L_{V,acc}}. \quad (27)$$

The above equation takes into account the increase in luminosity of the progenitor galaxy and luminosity of its GCS as a consequence of the accretion. Assuming that the accretion process occurs in a dissipationless way (i.e. no new stars or GCs are formed) and that no GCs are destroyed, the number of accreted galaxies can be expressed with the following relation:

$$N_{acc} = \frac{\Delta S_{LV}}{S_{LV,acc} - S_{LV,prg} - \Delta S_{LV}} \times \frac{L_{V,prg}}{L_{V,acc}}, \quad (28)$$

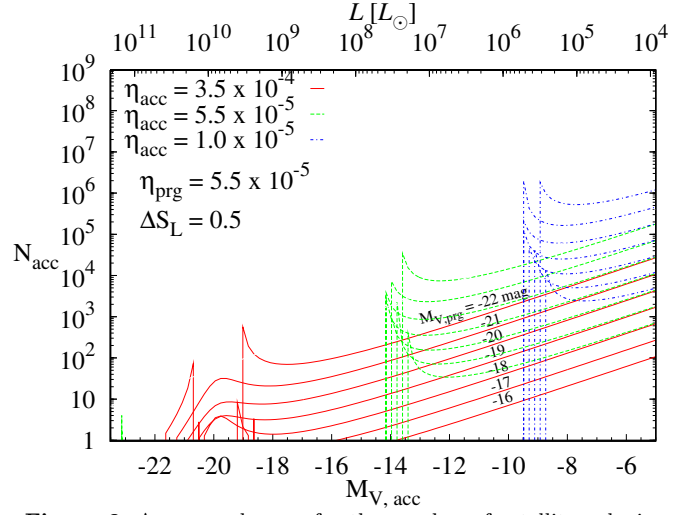


Figure 9. An example case for the number of satellite galaxies necessary to boost the specific luminosity of a host galaxy by $\Delta S_L = 0.5$ as a function of satellite luminosity, $M_{V,acc}$. The relations are parametrized by the luminosity of the progenitor galaxy, $M_{V,prg}$. The different line-types show three different cases of GC formation efficiencies of the accreted satellite galaxy (η_{acc}). The peaks and "knees" in the curves are caused by the inflection point of the "U-shaped" GC system scaling relations (cf. Fig. 6).

where $S_{L_{V,prg}}$, $L_{V,prg}$ and $S_{L_{V,acc}}$, $L_{V,acc}$ are the progenitor and accreted galaxy specific luminosity and brightness, respectively. The increase in the GC system specific luminosity due to dissipationless accretion of satellite galaxies is $\Delta S_{LV} = S_{L,V} - S_{L_{V,prg}}$. $S_{L,V}$ is the specific luminosity of the remnant galaxy after the accretion processes ended. Relation 28 gives the prescription to compute the number of accreted satellite galaxies with a given luminosity and η_{acc} (cf. top left panel of Figure 6) necessary to increase S_L by ΔS_L . To illustrate relation (28), we show in Figure 9 an example case for a progenitor galaxy with increased S_L value by $\Delta S_L = 0.5$ for three different η_{acc} values of the satellite galaxies and progenitor luminosities in the range $M_{V,prg} = -16$ to -22 mag. The shape and slope of the curves is a direct reflection of the functional relation between the S_L value and galaxy luminosity observed in Figure 6 and described by eq. (24) (see also Eq. A28). The only purpose of this simple example is to show that in the formalism of the current model an accretion of low-luminosity dwarfs with high S_L values can increase the S_L of a more massive progenitor galaxy. However, only a more detailed treatment with sampling an evolving galaxy luminosity function will yield realistic number estimates of accreted satellite galaxies distributed over a mass spectrum, which is beyond the scope of this study.

Thus, in this simplistic merging picture the accretion of a reasonable number of intermediate-luminosity, high- S_L dwarf galaxies offers a valid mechanism for boosting the GC system scaling parameters of cD galaxies. The observed correlation between the S_N of the cD galaxy and the X-ray flux of the host cluster Blakeslee (1999) supports this picture. Accretion and galaxy merging in the cluster core heats up the gas leading to the high X-ray flux. Such accretion and hierarchical growth of cD galaxies is also evidenced by the steepening of the faint-end slope of the luminosity

function of galaxies in galaxy clusters with increasing redshift (e.g., Ryan et al. 2007; Khochfar et al. 2007). In addition, the fraction of low-mass peculiar/irregular galaxies increases with redshift (e.g., Renzini 2006; Conselice et al. 2008). Moreover, observations of low-redshift Abell galaxy clusters show that galaxy clusters which host cD galaxies have smaller dwarf-to-giant ratios than non-cD clusters (Lopez-Cruz et al. 1997) and a clear radial dependence of the faint-end slope of the galaxy luminosity function becoming steeper in the cluster outskirts (Barkhouse et al. 2007). It therefore seems that the contribution of low-mass dwarfs to the buildup of the GC system of the most massive galaxies is likely non-negligible, especially at high redshifts. In fact, stripping of GCs from present-day dwarf galaxies in the cluster environment is suggested by the lack of any detectable GC systems around few dEs closest to M 87 and M 49 in the Virgo galaxy cluster (Peng et al. 2008). In the context of the current cosmological Λ CDM paradigm of structure formation (e.g., White & Rees 1978), it is of great importance to quantify the accreted mass fractions of GCs and field stars. It would be highly desirable to study the formation and enrichment timescales of the low and high- η dwarf galaxies in more detail and compare the field stellar populations in such galaxies with those of their GC systems.

5 CONCLUSIONS

We investigate the much debated behavior of the observed GCS scaling parameters as a function of galaxy luminosity, such as the GC specific frequency (S_N), specific luminosity (S_L), specific mass (S_M), and specific number (\dot{T}). Those are the integrated number, luminosity mass and specific number of all globular clusters in a galaxy normalized to the total galaxy luminosity and/or mass, respectively (see Sect. 3). We derive these quantities from *HST/ACS* data of low-mass, faint ($M_V > -16$ mag) dwarf galaxies, mainly late-type irregulars, located in the halo regions of nearby (< 10 Mpc) galaxy groups and in the field (Georgiev et al. 2008, 2009a). In order to investigate the scaling relations of their GCSs as a function of galaxy luminosity (mass) we also compiled data from the literature for massive cluster ellipticals (Peng et al. 2008) and spiral galaxies (Spitler et al. 2008). To complement our data in the low-mass regime we included 69 cluster dEs (Miller & Lotz 2007) and 12 dIrrs from Seth et al. (2004) and Georgiev et al. (2006), as well as 24 late-type dwarfs in the local low-density environment from Sharina et al. (2005). Thus, we cover virtually the entire range in galaxy luminosity from $M_V = -11$ to -23 mag ($10^6 - 10^{11} L_\odot$) where old GCs ($t \gtrsim 4$ Gyr) are reliably detected. Our main results can be summarized as follows:

- *Trends in GCS scaling relations hold irrespective of galaxy morphology.* — The significantly increased number of galaxies in our analysis in comparison with earlier studies over the entire mass and galaxy morphology range allowed us to firmly corroborate the previous observational findings that the GCS scaling parameters vary as a function of galaxy luminosity (Fig. 6). We find that this relation holds irrespective of galaxy morphological type, suggesting a universal mode of GC formation. Galaxies show increasing GCS scaling parameters toward low and high-luminosity

systems with a minimum at around $M_V \approx -20.5$ mag ($L_V \approx 2 \times 10^{10} L_\odot$).

- *S_L values of early-type galaxies are twice that of late-types at a given galaxy luminosity.* — The specific luminosity S_L is the most robust scaling parameter and shows least scatter due to its independence of distance and weak sensitivity to completeness corrections at the faint end slope of the GC luminosity function (Sect. 3.2.2). For late-type galaxies, spirals and irregulars the S_L value is on average two times smaller at a given galaxy luminosity than that for early-type systems (cf. Fig. 4). This difference can be partially accounted for by the passive evolutionary fading of the integrated galaxy light ($\Delta V \gtrsim 1$ mag), provided no more GCs are formed or destroyed at the same time (cf. arrow in Fig. 4). As cluster dSphs are on average fainter and exhibit higher scaling parameters than field dIrrs, the above analysis supports the idea that dIrr galaxies could be the progenitors of dSphs and fainter dEs (e.g. Miller et al. 1998), but see also Grebel et al. (2003). However, our sample contains mostly dIrrs in field and group environments. Their GC scaling parameters might differ in cluster environments due to varying GC formation efficiencies and/or cluster stripping. However, such cluster dIrrs have not been sampled well enough yet.

- *The "U-shaped" behavior of the GC scaling parameters is remarkably well described by a two component model at a transitional halo mass critical for the thermal properties of the inflowing gas.* — In order to explain the trends in the GCS scaling parameters we have assumed that the total mass in GCs is proportional to the total halo mass of the host galaxy ($\mathcal{M}_{\text{GCS}} = \eta \mathcal{M}_h$), i.e. the formation of GCs scales with the total galaxy mass. The coefficient, η , is the *specific GC formation efficiency* parameter, which measures the present-day mass/luminosity of the GCS drawn from the initial star cluster population mass/luminosity function shaped by various mechanisms over a Hubble time (cluster relaxation, tidal and dynamical friction, dissolution). We have invoked theoretical models of Dekel & Birnboim (2006) which predict the dependence of the galaxy \mathcal{M}/L as a function of galaxy mass determined by the thermal properties of the inflowing gas for two different halo mass regimes in which star formation processes are regulated by supernova feedback and virial shocks below and above the critical stellar mass of $3 \times 10^{10} \mathcal{M}_\odot$. For low-mass halos these models predict that the mass-to-light ratio varies with host galaxy mass as $\mathcal{M}_h/L \propto \mathcal{M}_h^{-2/3}$ (see also Dekel & Silk 1986). To draw quantitative conclusions, the absolute normalization of this relation is very important which we derive from recent observations of the mass in the inner 0.3 kpc ($\mathcal{M}_{0.3} = 10^7 \mathcal{M}_\odot$) of nearby low-mass dwarf galaxies (Strigari et al. 2008) using its relation to the total halo mass from the models of Bullock et al. (2001). Above the critical mass, at large halo masses the models predict $\mathcal{M}_h/L \propto \mathcal{M}_h^{1/2}$ which we calibrate with dynamical mass measurements based on galactic group dynamics of massive early-type galaxies (Eke et al. 2006). This results in an analytical model which describes remarkably well the observed trends in the GC scaling relations as a function of galaxy luminosity (Sect 4.2.2). In the Dekel & Birnboim (2006) model, compact and dense molecular clouds (the

sites of GC formation) are efficiently shielded against shock heating and ionizing stellar feedback above and below the critical galaxy mass, respectively. This implies that in this picture, the shape of the GC scaling relations can be described as a universal GC formation efficiency for the entire galaxy mass range but with an evolving field star-formation efficiency. The latter is equally low for low- and high-mass systems (compared to the formation of massive/dense star clusters) due to being efficiently suppressed by the stellar and SNe ionizing feedback and shock heating of the inflowing gas below and above the critical galaxy mass ($\sim 10^{10.5} M_{\odot}$), respectively. This causes an evolution of the mass in clusters to mass in field stars ratio as a function of galaxy mass. The evolution of this ratio is at the roots of the shape of the GC scaling relations. The best fit of this model to the observed distributions yielded a value of the observed GC formation efficiency parameter (η) for the luminosity and mass-normalized GC formation efficiency of $\langle \eta_L \rangle \simeq 5.5 \times 10^{-5}$ and $\langle \eta_M \rangle \simeq 6.47 \times 10^{-5}$ (see Sect. 4.3). The η distributions are very similar for all galaxy types, if passive evolutionary fading of the late-type galaxy sample of ~ 1 mag is applied (cf. Fig. 8).

- *The differences between model predictions and observations can be attributed to a mixture of effects of varying GC formation efficiencies, galaxy merging histories, and a variation in cluster destruction mechanisms as a function of galaxy mass lacking in the current model.* — The most massive galaxies, whose S_M and S_L values increase more rapidly than expected from the theoretical predictions for a fixed η can be understood as systems which have either undergone an early episode of extremely efficient star-cluster formation or less efficient formation of field stars or which have preferentially accreted high- η dwarf galaxies. In a simple merging picture of satellite galaxies of a given luminosity we showed in Sect. 4.4 that it is possible to boost the S_L values of galaxies by accretion of intermediate luminosity, high- η dwarfs, thus offering an efficient mechanism for explaining the high η values of cD galaxies. In addition, the observed spread in η may be caused by the stochastic nature of star and star-cluster formation at low galaxy mass or by differences in SFH and SFR intensity for galaxies at the same luminosity.

To understand whether the difference in the GCS scaling-parameter (S_L or S_M) distributions between late- and early-type galaxies is statistically significant and, if so, to understand the nature of this difference (e.g. age, chemical enrichment, environment, etc.) it is crucial to sample with more observations (e.g. near-UV/IR photometry or spectroscopy) the GCSs of spiral galaxies at intermediate to high masses, late-type dwarfs in dense cluster environments, both of which are significantly under represented in the current study.

ACKNOWLEDGMENTS

IG is thankful for the financial support through German Research Foundation (*Deutsche Forschungsgemeinschaft, DFG*) grant DFG-Projekt BO-779/32-1 and by the STScI Director's Discretionary Research Fund. THP gratefully ac-

knowledges support from the National Research Council of Canada in form of the Plaskett Research Fellowship. The authors would like to thank Tom Richtler for providing comments to an earlier version of this paper as well as Eric Peng and Knut Olsen for valuable comments and suggestions. The authors thank the referee for the constructive input which improved the paper.

REFERENCES

- Anders, P. & Fritze-v. Alvensleben, U. 2003, *A&A*, 401, 1063
- Ashman, K. M. & Zepf, S. E. 1992, *ApJ*, 384, 50
- Ashman, K. M. & Zepf, S. E. 1998, *Globular Cluster Systems* (Cambridge University Press, 1998. (Cambridge astrophysics series ; 30) QB853.5 .A84 1998)
- Barkhouse, W. A., Yee, H. K. C., & López-Cruz, O. 2007, *ApJ*, 671, 1471
- Bassino, L. P., Faifer, F. R., Forte, J. C., et al. 2006a, *A&A*, 451, 789
- Bassino, L. P., Richtler, T., & Dirsch, B. 2006b, *MNRAS*, 367, 156
- Bassino, L. P., Richtler, T., & Dirsch, B. 2008, *MNRAS*, 386, 1145
- Bastian, N. 2008, *MNRAS*, 390, 759
- Begum, A., Chengalur, J. N., Karachentsev, I. D., Sharina, M. E., & Kaisin, S. S. 2008, *MNRAS*, 386, 1667
- Bekki, K., Yahagi, H., & Forbes, D. A. 2006, *ApJL*, 645, L29
- Bell, E. F., McIntosh, D. H., Katz, N., & Weinberg, M. D. 2003, *ApJS*, 149, 289
- Belokurov, V., Zucker, D. B., Evans, N. W., et al. 2007, *ApJ*, 654, 897
- Belokurov, V., Zucker, D. B., Evans, N. W., et al. 2006, *ApJL*, 647, L111
- Blakeslee, J. P. 1999, *AJ*, 118, 1506
- Blakeslee, J. P., Tonry, J. L., & Metzger, M. R. 1997, *AJ*, 114, 482
- Brodie, J. P. & Strader, J. 2006, *ARA&A*, 44, 193
- Bruzual, G. & Charlot, S. 2003, *MNRAS*, 344, 1000
- Bullock, J. S., Kolatt, T. S., Sigad, Y., et al. 2001, *MNRAS*, 321, 559
- Chandar, R., Whitmore, B., & Lee, M. G. 2004, *ApJ*, 611, 220
- Conselice, C. J., Rajgor, S., & Myers, R. 2008, *MNRAS*, 446
- Côté, P., Marzke, R. O., & West, M. J. 1998, *ApJ*, 501, 554
- Côté, P., West, M. J., & Marzke, R. O. 2002, *ApJ*, 567, 853
- Cox, A. N. 2000, *Allen's astrophysical quantities* (Allen's Astrophysical Quantities)
- Crnojević, D., Grebel, E. K., & Koch, A. 2010, *ArXiv:1002.0341*
- Dahlem, M., Lisenfeld, U., & Rossa, J. 2006, *A&A*, 457, 121
- Dekel, A. & Birnboim, Y. 2006, *MNRAS*, 368, 2
- Dekel, A. & Silk, J. 1986, *ApJ*, 303, 39
- Dekel, A. & Woo, J. 2003, *MNRAS*, 344, 1131
- Dirsch, B., Richtler, T., Geisler, D., et al. 2003, *AJ*, 125, 1908
- Dirsch, B., Schuberth, Y., & Richtler, T. 2005, *A&A*, 433, 43

- Durrell, P. R., Harris, W. E., Geisler, D., & Pudritz, R. E. 1996, *AJ*, 112, 972
- Eke, V. R., Baugh, C. M., Cole, S., Frenk, C. S., & Navarro, J. F. 2006, *MNRAS*, 370, 1147
- Elmegreen, B. G. 2010, *ApJL*, 712, L184
- Fall, S. M. & Zhang, Q. 2001, *ApJ*, 561, 751
- Forbes, D. A. 2005, *ApJL*, 635, L137
- Forbes, D. A. & Bridges, T. 2010, *ArXiv:1001.4289*
- Forbes, D. A., Brodie, J. P., & Grillmair, C. J. 1997, *AJ*, 113, 1652
- Forbes, D. A., Georgakakis, A. E., & Brodie, J. P. 2001, *MNRAS*, 325, 1431
- Forte, J. C., Geisler, D., Ostrov, P. G., Piatti, A. E., & Gieren, W. 2001, *AJ*, 121, 1992
- Fukazawa, Y., Botoya-Nonesá, J. G., Pu, J., Ohto, A., & Kawano, N. 2006, *ApJ*, 636, 698
- Georgiev, I. Y., Goudfrooij, P., Puzia, T. H., & Hilker, M. 2008, *AJ*, 135, 1858
- Georgiev, I. Y., Hilker, M., Puzia, T. H., et al. 2006, *A&A*, 452, 141
- Georgiev, I. Y., Puzia, T. H., Hilker, M., & Goudfrooij, P. 2009a, *MNRAS*, 392, 879
- Georgiev, I. Y., sHilker, M., Puzia, T. H., Goudfrooij, P., & Baumgardt, H. 2009b, *MNRAS*, 396, 1075
- Giavalisco, M., Ferguson, H. C., Koekemoer, A. M., et al. 2004, *ApJL*, 600, L93
- Gieles, M. & Bastian, N. 2008, *A&A*, 482, 165
- Gieles, M., Portegies Zwart, S. F., Baumgardt, H., et al. 2006, *MNRAS*, 371, 793
- Gómez, M. & Richtler, T. 2004, *A&A*, 415, 499
- Goudfrooij, P., Gilmore, D., Whitmore, B. C., & Schweizer, F. 2004, *ApJ*, 613, L121
- Goudfrooij, P., Schweizer, F., Gilmore, D., & Whitmore, B. C. 2007, *AJ*, 133, 2737
- Goudfrooij, P., Strader, J., Brenneman, L., et al. 2003, *MNRAS*, 343, 665
- Grebel, E. K., Gallagher, III, J. S., & Harbeck, D. 2003, *AJ*, 125, 1926
- Harris, W. E. 1991, *ARA&A*, 29, 543
- Harris, W. E. 2001, in *Saas-Fee Advanced Course 28: Star Clusters*, ed. L. Labhardt & B. Binggeli, 223–+
- Harris, W. E. 2003, in *Extragalactic Globular Cluster Systems*, ed. M. Kissler-Patig, 317–+
- Harris, W. E. & Harris, G. L. H. 2002, *AJ*, 123, 3108
- Harris, W. E., Kavelaars, J. J., Hanes, D. A., Pritchett, C. J., & Baum, W. A. 2009, *AJ*, 137, 3314
- Harris, W. E. & van den Bergh, S. 1981, *AJ*, 86, 1627
- Harris, W. E., Whitmore, B. C., Karakla, D., et al. 2006, *ApJ*, 636, 90
- Hilker, M., Infante, L., & Richtler, T. 1999, *A&AS*, 138, 55
- Hinshaw, G., Weiland, J. L., Hill, R. S., et al. 2009, *ApJS*, 180, 225
- Humphrey, P. J., Buote, D. A., Gastaldello, F., et al. 2006, *ApJ*, 646, 899
- Irwin, M. J., Belokurov, V., Evans, N. W., et al. 2007, *ApJL*, 656, L13
- Jordán, A., McLaughlin, D. E., Côté, P., et al. 2007, *ApJS*, 171, 101
- Karachentsev, I. D., Dolphin, A., Tully, R. B., et al. 2006, *AJ*, 131, 1361
- Karachentsev, I. D., Tully, R. B., Dolphin, A., et al. 2007, *AJ*, 133, 504
- Khochfar, S., Silk, J., Windhorst, R. A., & Ryan, Jr., R. E. 2007, *ApJL*, 668, L115
- Kissler-Patig, M. 2000, in *Reviews in Modern Astronomy*, ed. R. E. Schielicke, 13–+
- Kravtsov, A. V. & Gnedin, O. Y. 2005, *ApJ*, 623, 650
- Kruijssen, J. M. D. & Portegies Zwart, S. F. 2009, *ApJL*, 698, L158
- Lada, C. J. & Lada, E. A. 2003, *ARA&A*, 41, 57
- Lamers, H. J. G. L. M. & Gieles, M. 2008, in *Astronomical Society of the Pacific Conference Series*, Vol. 388, *Mass Loss from Stars and the Evolution of Stellar Clusters*, ed. A. de Koter, L. J. Smith, & L. B. F. M. Waters, 367–+
- Larsen, S. S. & Richtler, T. 2000, *A&A*, 354, 836
- Leitherer, C., Schaerer, D., Goldader, J. D., et al. 1999, *ApJS*, 123, 3
- Lianou, S., Grebel, E. K., & Koch, A. 2010, *ArXiv:1003.0861*
- Lopez-Cruz, O., Yee, H. K. C., Brown, J. P., Jones, C., & Forman, W. 1997, *ApJL*, 475, L97+
- Maraston, C. 2005, *MNRAS*, 362, 799
- Mateo, M. L. 1998, *ARA&A*, 36, 435
- McLaughlin, D. E. 1999, *AJ*, 117, 2398
- McLaughlin, D. E. & Fall, S. M. 2008, *ApJ*, 679, 1272
- McLaughlin, D. E. & van der Marel, R. P. 2005, *ApJS*, 161, 304
- Miller, B. W. & Lotz, J. M. 2007, *ApJ*, 670, 1074
- Miller, B. W., Lotz, J. M., Ferguson, H. C., Stiavelli, M., & Whitmore, B. C. 1998, *ApJL*, 508, L133
- Muratov, A. L. & Gnedin, O. Y. 2010, *ArXiv:1002.1325*
- Olsen, K. A. G., Miller, B. W., Suntzeff, N. B., Schommer, R. A., & Bright, J. 2004, *AJ*, 127, 2674
- O’Sullivan, E., Sanderson, A. J. R., & Ponman, T. J. 2007, *MNRAS*, 380, 1409
- Parmentier, G. 2009, *ArXiv:0901.3140*
- Parmentier, G. & Fritze, U. 2009, *ApJ*, 690, 1112
- Paturel, G., Petit, C., Prugniel, P., et al. 2003, *A&A*, 412, 45
- Peng, E. W., Jordán, A., Côté, P., et al. 2006, *ApJ*, 639, 95
- Peng, E. W., Jordan, A., Cote, P., et al. 2008, *astro-ph/0803.0330*, 803
- Pipino, A., Puzia, T. H., & Matteucci, F. 2007, *ApJ*, 665, 295
- Puzia, T. H. & Sharina, M. E. 2008, *ApJ*, 674, 909
- Renzini, A. 2006, *ARA&A*, 44, 141
- Rhode, K. L. & Zepf, S. E. 2001, *AJ*, 121, 210
- Rhode, K. L. & Zepf, S. E. 2003, *AJ*, 126, 2307
- Rhode, K. L. & Zepf, S. E. 2004, *AJ*, 127, 302
- Rhode, K. L., Zepf, S. E., Kundu, A., & Larner, A. N. 2007, *AJ*, 134, 1403
- Rhode, K. L., Zepf, S. E., & Santos, M. R. 2005, *ApJL*, 630, L21
- Roberts, M. S. & Haynes, M. P. 1994, *ARA&A*, 32, 115
- Ryan, R. E. J., Hathi, N. P., Cohen, S. H., et al. 2007, *ApJ*, 668, 839
- Schlegel, D. J., Finkbeiner, D. P., & Davis, M. 1998, *ApJ*, 500, 525
- Seth, A., Olsen, K., Miller, B., Lotz, J., & Telford, R. 2004, *AJ*, 127, 798
- Sharina, M. E., Chandar, R., Puzia, T. H., Goudfrooij, P., & Davoust, E. 2010, *ArXiv:1002.2144*

- Sharina, M. E., Puzia, T. H., & Makarov, D. I. 2005, *A&A*, 442, 85
- Spitler, L. R. & Forbes, D. A. 2009, *MNRAS*, 392, L1
- Spitler, L. R., Forbes, D. A., Strader, J., Brodie, J. P., & Gallagher, J. S. 2008, *MNRAS*, 385, 361
- Strader, J., Brodie, J. P., Spitler, L., & Beasley, M. A. 2006, *AJ*, 132, 2333
- Strigari, L. E., Bullock, J. S., Kaplinghat, M., et al. 2008, *Nature*, 454, 1096
- Tamura, N., Sharples, R. M., Arimoto, N., et al. 2006a, *MNRAS*, 373, 588
- Tamura, N., Sharples, R. M., Arimoto, N., et al. 2006b, *MNRAS*, 373, 601
- Tully, R. B., Rizzi, L., Dolphin, A. E., et al. 2006, *AJ*, 132, 729
- van den Bergh, S. 2000, *PASP*, 112, 932
- van den Bergh, S. & Mackey, A. D. 2004, *MNRAS*, 354, 713
- Vesperini, E. 1998, *MNRAS*, 299, 1019
- Vesperini, E. 2000, *MNRAS*, 318, 841
- Walsh, S. M., Jerjen, H., & Willman, B. 2007, *ApJL*, 662, L83
- Wehner, E., Harris, B., Whitmore, B., Rothberg, B., & Woodley, K. 2008, *astro-ph/0802.1723*, 802
- Weisz, D. R., Skillman, E. D., Cannon, J. M., et al. 2008, *ApJ*, 689, 160
- West, M. J., Cote, P., Jones, C., Forman, W., & Marzke, R. O. 1995, *ApJL*, 453, L77+
- White, S. D. M. & Rees, M. J. 1978, *MNRAS*, 183, 341
- Whitmore, B. C. & Schweizer, F. 1995, *AJ*, 109, 960
- Whitmore, B. C., Zhang, Q., Leitherer, C., et al. 1999, *AJ*, 118, 1551
- Willman, B., Blanton, M. R., West, A. A., et al. 2005a, *AJ*, 129, 2692
- Willman, B., Dalcanton, J. J., Martinez-Delgado, D., et al. 2005b, *ApJL*, 626, L85
- Zepf, S. E. & Ashman, K. M. 1993, *MNRAS*, 264, 611
- Zucker, D. B., Belokurov, V., Evans, N. W., et al. 2006a, *ApJL*, 650, L41
- Zucker, D. B., Belokurov, V., Evans, N. W., et al. 2006b, *ApJL*, 643, L103

Table 1. Properties of the globular cluster systems of the studied dwarf galaxies

Galaxy	Type T-value (2)	M_V [mag] (3)	$M/L_{V,Gal}$	$M_{*,V,Gal}$ $10^7 M_\odot$ (5)	M_{HI} $10^7 M_\odot$ (6)	N_{blue} (7)	N_{tot} (8)	M_{blue} $10^4 M_\odot$ (9)	M_{tot} $10^4 M_\odot$ (10)	$S_{N,tot}$ (11)	S_L (12)	S_M (13)	\hat{T} (14)	$\log \eta_L$ (15)	$\log \eta_M$ (16)
D634-03	10.0 I	-11.94	0.691	0.35	0.49	0	1	0.00	10.82	16.75	1.14	1.29	119.05	-4.39	-4.77
DDO52	10.0 Im	-14.98	0.767	6.38	19.99	1	2	10.52	17.61	2.04	0.11	0.07	7.58	-4.91	-5.52
ESO 059-01	10.0 IBsm	-14.60	0.867	5.08	8.26	1	1	143.93	143.93	1.45	1.31	1.08	7.50	-3.90	-4.32
ESO 121-20	10.0 Im	-13.64	0.404	0.98	11.49	0	1	0.00	4.04	3.50	0.09	0.03	8.02	-5.22	-6.33
ESO 137-18	5.0 SAsc	-17.21	1.049	68.04	34.14	4	7	69.69	111.20	0.91	0.09	0.11	6.85	-4.65	-4.82
ESO 154-023	8.9 SBsm	-16.38	0.662	19.99	81.70	0	3	0.00	3.52	0.84	0.01	0.00	2.95	-5.94	-6.65
ESO 223-09	9.7 IAB	-16.47	0.691	22.67	63.89	6	8	210.46	307.84	2.07	0.50	0.36	9.24	-4.02	-4.61
ESO 269-58	-2.2 I0	-15.78	1.732	30.10	2.31	6	8	76.97	76.97	3.90	0.24	0.24	24.68	-4.46	-4.49
ESO 269-66	-5.0 dE,N	-13.89	0.986	3.01	0.00	3	4	196.86	224.63	11.12	3.92	7.48	133.11	-3.54	-3.54
ESO 274-01	6.6 Scd	-17.47	1.834	151.15	20.18	3	10	41.31	130.61	1.03	0.08	0.08	5.84	-4.64	-4.70
ESO 349-031	10.0 IBm	-11.87	0.629	0.30	1.34	0	1	0.00	2.74	17.86	0.31	0.17	61.05	-4.97	-5.71
ESO 381-20	9.8 IBsm	-14.80	0.766	5.40	15.77	0	1	0.00	2.28	1.20	0.02	0.01	4.72	-5.75	-6.34
ESO 384-016	-5 dSO/Im	-13.72	0.691	1.80	0.50	0	2	0.00	5.83	6.50	0.12	0.25	86.92	-5.08	-5.19
IC 1959	8.4 SBsm	-15.99	0.672	14.17	18.73	4	7	159.26	172.34	2.81	0.44	0.52	21.28	-4.16	-4.53
IKN	? dSph	-11.51	0.691	0.24	0.00	4	5	72.40	80.46	124.44	12.57	34.24	2127.66	-3.41	-3.41
KK 16	10.0 I	-12.38	0.691	0.52	0.69	0	1	0.00	2.08	11.17	0.15	0.17	82.37	-5.21	-5.58
KK 17	10.0 I	-10.57	0.691	0.10	0.55	0	1	0.00	1.09	59.16	0.41	0.17	154.08	-5.06	-5.87
KK 197	10.0 Im	-13.04	0.691	0.96	0.00	2	3	148.96	151.97	18.24	5.80	15.78	311.53	-3.51	-3.51
KK 246	10.0 I	-13.77	0.354	0.97	11.92	2	2	41.04	41.04	6.21	0.80	0.32	15.52	-4.25	-5.37
KK 27	10.0 I	-10.14	0.691	0.07	0.00	0	2	0.00	6.03	175.80	3.33	9.00	2985.07	-4.21	-4.21
KKH 77	10.0 I	-14.58	0.691	3.98	4.67	1	2	24.78	27.11	2.94	0.25	0.31	23.13	-4.62	-4.96
KKS 55	- dSph	-11.17	0.691	0.17	0.00	1	1	14.00	14.00	34.04	2.99	8.14	581.40	-4.09	-4.09
NGC 1311	8.7 SBm	-15.76	0.691	11.79	8.74	3	5	63.64	68.31	2.48	0.21	0.33	24.36	-4.51	-4.75
NGC 247	6.9 SABd	-18.76	0.860	232.54	137.06	1	25	14.80	398.20	0.78	0.08	0.11	6.76	-4.50	-4.70
NGC 4163	9.9 I	-14.21	0.469	1.92	1.42	2	2	111.57	111.57	4.14	1.45	3.34	59.90	-3.92	-4.16
NGC 4605	5.0 SBd	-18.41	0.883	172.97	25.88	7	22	85.92	350.41	0.95	0.10	0.18	11.06	-4.46	-4.52
NGC 5237	- I?	-15.45	1.211	15.53	3.10	2	3	47.32	53.21	1.98	0.22	0.29	16.10	-4.54	-4.62
NGC 784	7.8 SBdm	-16.87	1.785	84.65	28.90	4	6	36.70	40.71	1.07	0.05	0.04	5.28	-5.00	-5.13
UGC 1281	7.5 Sdm	-15.30	1.134	12.67	16.49	1	2	17.30	31.95	1.52	0.15	0.11	6.86	-4.73	-5.09
UGC 3755	9.9 Im	-15.50	0.691	9.28	13.95	6	9	174.20	239.30	5.68	0.95	1.03	38.74	-3.90	-4.30
UGC 3974	9.8 IBm	-15.33	0.691	7.93	63.75	4	4	118.66	118.66	2.95	0.55	0.17	5.58	-4.01	-4.97
UGC 4115	9.9 Im	-15.12	0.900	8.52	20.95	1	5	17.79	29.86	4.48	0.17	0.10	16.97	-4.71	-5.25
UGC 685	9.2 Im	-14.35	0.691	3.22	5.88	5	5	136.93	136.93	9.10	1.56	1.51	54.96	-3.86	-4.32
UGC 7369	-3 dSph	-16.17	0.691	17.20	0.00	14	22	1208.08	1255.32	7.49	2.68	7.30	127.92	-3.34	-3.34
UGC 8638	9.9 Im	-13.69	0.641	1.63	1.17	2	3	26.27	246.14	10.03	5.16	8.81	107.33	-3.45	-3.69
UGC 8760	9.8 IBm	-13.16	0.691	1.08	1.86	0	1	0.00	1.33	5.45	0.05	0.05	34.07	-5.59	-6.03

Table 1 (cont'd)

Galaxy (1)	Type T-value (2)	M_V [mag] (3)	$M/L_V, \text{Gal}$ (4)	$M_{*,V, \text{Gal}}$ $10^7 M_\odot$ (5)	M_{HI} $10^7 M_\odot$ (6)	N_{blue} (7)	N_{tot} (8)	M^{blue} $10^4 M_\odot$ (9)	M_{tot} $10^4 M_\odot$ (10)	$S_{N, \text{tot}}$ (11)	S_L (12)	S_M (13)	\hat{T} (14)	$\log \eta_L$ (15)	$\log \eta_M$ (16)
UGCA 86	9.9 Im	-16.13	0.691	16.58	48.25	10	11	685.29	1148.91	3.89	2.55	1.77	16.97	-3.37	-3.96
UGCA 92	10.0 Im	-14.71	0.691	4.48	7.62	1	2	19.87	46.06	2.61	0.38	0.38	16.53	-4.42	-4.86
LMC	9.1 I	-18.36	0.870	162.75	44.12	16	16	330.27	330.27	0.72	0.09	0.16	7.73	-4.47	-4.57
SMC	8.9 I	-16.82	0.815	36.91	51.20	1	1	32.16	32.16	0.19	0.04	0.04	1.13	-5.09	-5.47
NGC1427A	9.9 IBsm	-18.50	0.937	199.41	176.63	38	38	605.26	605.26	1.66	0.15	0.16	10.11	-4.24	-4.52

Note. — Columns (1) through (6) contain the galaxy ID, morphological classification as listed in HyperLEDA and NED, its absolute magnitude, $V-I$ band mass-to-light ratio (see Sect. 3.2), stellar mass and HI mass (see Sect. 3.2), respectively. In columns (7) through (10) is the number of "blue" GCs $0.7 < V-I < 1.0$ mag, the total number of GCs in the galaxy, the mass of the blue GCs and the total mass of the GC system, respectively. In column (11) is the GC specific frequency, in (12) specific luminosity, (13) specific mass and in (14) number of GCs normalized to the galaxy mass. The logarithm of the luminosity and mass normalized GC formation efficiencies are shown in columns (15) and (16), respectively (see Sect. 4.3).

APPENDIX A: SCALING RELATIONS OF GC SYSTEMS AS A FUNCTION OF GALAXY MASS (DARK AND BARYON) AND LUMINOSITY

A1 GCSs scaling relations in the "SNe feedback" galaxy mass regime

Using Equations (9) through (11) we express Equations (2), (3), and (4) as a function of galaxy luminosity, total halo and baryon mass for $\mathcal{M}_h < 3 \times 10^{10} M_\odot$.

$$\log S_N = 6 + 0.4M_{V,\odot} + \log\left(\frac{\eta\kappa_1^{0.6}}{m_{\text{TO}}}\right) - 0.4 \log L_V \quad (\text{A1})$$

$$= 6 + 0.4M_{V,\odot} + \log\left(\frac{\eta\kappa_1}{m_{\text{TO}}}\right) - \frac{2}{3} \log \mathcal{M}_h \quad (\text{A2})$$

$$= 6 + 0.4M_{V,\odot} + \log\left(\frac{\eta}{m_{\text{TO}}}\frac{\kappa_1^{0.6}}{\Upsilon_V^{0.6}}\right) - 0.4 \log \mathcal{M}_b \quad (\text{A3})$$

$$\log S_L = 2 + \log\left(\frac{\eta\kappa_1^{0.6}}{\gamma_V}\right) - 0.4 \log L_V \quad (\text{A4})$$

$$= 2 + \log\left(\frac{\eta\kappa_1}{\gamma_V}\right) - \frac{2}{3} \log \mathcal{M}_h \quad (\text{A5})$$

$$= 2 + \log\left(\frac{\eta\kappa_1^{0.6}\Upsilon_V^{0.4}}{\gamma_V}\right) - 0.4 \log \mathcal{M}_b \quad (\text{A6})$$

$$\log S_M = 2 + \log\left(\frac{\eta\kappa_1^{0.6}}{\Upsilon_V}\right) - 0.4 \log L_V \quad (\text{A7})$$

$$= 2 + \log\left(\frac{\eta\kappa_1}{\Upsilon_V}\right) - \frac{2}{3} \log \mathcal{M}_h \quad (\text{A8})$$

$$= 2 + \log\left(\eta\frac{\kappa_1^{0.6}}{\Upsilon_V^{0.6}}\right) - 0.4 \log \mathcal{M}_b \quad (\text{A9})$$

$$\log \hat{T} = 9 + \log\left(\frac{\eta\kappa_1^{0.6}}{\Upsilon_V m_{\text{TO}}}\right) - 0.4 \log L_V \quad (\text{A10})$$

$$= 9 + \log\left(\frac{\eta\kappa_1}{\Upsilon_V m_{\text{TO}}}\right) - \frac{2}{3} \log \mathcal{M}_h, \quad (\text{A11})$$

$$= 9 + \log\left(\frac{\eta\kappa_1^{0.6}}{m_{\text{TO}}\Upsilon_V^{0.6}}\right) - 0.4 \log \mathcal{M}_b, \quad (\text{A12})$$

A2 GCSs scaling relations in the "Virial-shock" galaxy mass regime

Using Equations (9) through (12) we express Equations (2), (3), and (4) as a function of galaxy luminosity, total halo and baryon mass for $\mathcal{M}_h > 3 \times 10^{10} M_\odot$.

$$\log S_N = 6 + 0.4M_{V,\odot} + \log\left(\frac{\eta\kappa_2^2}{m_{\text{TO}}}\right) + 1.2 \log L_V \quad (\text{A13})$$

$$= 6 + 0.4M_{V,\odot} + \log\left(\frac{\eta\kappa_2^{-0.8}}{m_{\text{TO}}}\right) + \frac{3}{5} \log \mathcal{M}_h \quad (\text{A14})$$

$$= 6 + 0.4M_{V,\odot} + \log\left(\frac{\eta\kappa_2^2}{m_{\text{TO}}\Upsilon_V^{1.2}}\right) + 1.2 \log \mathcal{M}_b \quad (\text{A15})$$

$$\log S_L = 2 + \log\left(\frac{\eta\kappa_2^2}{\gamma_V}\right) + \log L_V \quad (\text{A16})$$

$$= 2 + \log\left(\frac{\eta\kappa_2}{\gamma_V}\right) + \frac{1}{2} \log \mathcal{M}_h \quad (\text{A17})$$

$$= 2 + \log\left(\frac{\eta\kappa_2^2}{\gamma_V\Upsilon_V}\right) + \log \mathcal{M}_b \quad (\text{A18})$$

$$\log S_M = 2 + \log\left(\frac{\eta\kappa_2^2}{\Upsilon_V}\right) + \log L_V \quad (\text{A19})$$

$$= 2 + \log\left(\frac{\eta\kappa_2}{\Upsilon_V}\right) + \frac{1}{2} \log \mathcal{M}_h \quad (\text{A20})$$

$$= 2 + \log\left(\frac{\eta\kappa_2^2}{\Upsilon_V^2}\right) + \log \mathcal{M}_b \quad (\text{A21})$$

$$\log \hat{T} = 9 + \log\left(\frac{\eta\kappa_2^2}{\Upsilon_V m_{\text{TO}}}\right) + \log L_V \quad (\text{A22})$$

$$= 9 + \log\left(\frac{\eta\kappa_2}{\Upsilon_V m_{\text{TO}}}\right) + \frac{1}{2} \log \mathcal{M}_h, \quad (\text{A23})$$

$$= 9 + \log\left(\frac{\eta}{m_{\text{TO}}}\frac{\kappa_2^2}{\Upsilon_V^2}\right) + \log \mathcal{M}_b, \quad (\text{A24})$$

A3 Continuous GCSs scaling relations from the "Virial-shock" to the "SNe feedback" galaxy mass regime

$$S_N = 10^{6+0.4M_{V,\odot}} \frac{\eta}{m_{\text{TO}}} (\kappa_1^{0.6} L_V^{-0.4} + \kappa_2^2 L_V^{1.2}) \quad (\text{A25})$$

$$= 10^{6+0.4M_{V,\odot}} \frac{\eta}{m_{\text{TO}}} (\kappa_1 \mathcal{M}_h^{-2/3} + \kappa_2^{-0.8} \mathcal{M}_h^{3/5}) \quad (\text{A26})$$

$$= 10^{6+0.4M_{V,\odot}} \frac{\eta}{m_{\text{TO}}} \left((\kappa_1 \Upsilon_V)^{0.6} \mathcal{M}_b^{-0.4} + \frac{\kappa_2^2}{\Upsilon_V^{1.2}} \mathcal{M}_b^{1.2} \right) \quad (\text{A27})$$

$$S_L = 10^2 \frac{\eta}{\gamma_V} (\kappa_1^{0.6} L_V^{-0.4} + \kappa_2^2 L_V) \quad (\text{A28})$$

$$= 10^2 \frac{\eta}{\gamma_V} (\kappa_1 \mathcal{M}_h^{-2/3} + \kappa_2 \mathcal{M}_h^{1/2}) \quad (\text{A29})$$

$$= 10^2 \frac{\eta}{\gamma_V} \left(\kappa_1^{0.6} \Upsilon_V^{0.4} \mathcal{M}_b^{-0.4} + \frac{\kappa_2^2}{\Upsilon_V} \mathcal{M}_b \right) \quad (\text{A30})$$

$$S_M = 10^2 \frac{\eta}{\Upsilon_V} (\kappa_1^{0.6} L_V^{-0.4} + \kappa_2^2 L_V) \quad (\text{A31})$$

$$= 10^2 \frac{\eta}{\Upsilon_V} (\kappa_1 \mathcal{M}_h^{-2/3} + \kappa_2 \mathcal{M}_h^{1/2}) \quad (\text{A32})$$

$$= 10^2 \eta \left(\left(\frac{\kappa_1}{\Upsilon_V} \right)^{0.6} \mathcal{M}_b^{-0.4} + \left(\frac{\kappa_2}{\Upsilon_V} \right)^2 \mathcal{M}_b \right) \quad (\text{A33})$$

$$\hat{T} = 10^9 \frac{\eta}{m_{\text{TO}}\Upsilon_V} (\kappa_1^{0.6} L_V^{-0.4} + \kappa_2^2 L_V) \quad (\text{A34})$$

$$= 10^9 \frac{\eta}{m_{\text{TO}}\Upsilon_V} (\kappa_1 \mathcal{M}_h^{-2/3} + \kappa_2 \mathcal{M}_h^{1/2}) \quad (\text{A35})$$

$$= 10^9 \frac{\eta}{m_{\text{TO}}} \left(\left(\frac{\kappa_2}{\Upsilon_V} \right)^{0.4} \mathcal{M}_b^{-0.4} + \left(\frac{\kappa_2}{\Upsilon_V} \right)^2 \mathcal{M}_b \right) \quad (\text{A36})$$